

Improving RCT-Based Treatment Effect Estimation Under Covariate Mismatch via Calibrated Alignment

Amir Asiaee*¹Samhita Pal¹¹Department of Biostatistics, Vanderbilt University Medical Center, TN 37203, USA

Abstract

Randomized controlled trials (RCTs) are the gold standard for estimating heterogeneous treatment effects, yet they are often underpowered for detecting effect heterogeneity. Large observational studies (OS) can supplement RCTs for conditional average treatment effect (CATE) estimation, but a key barrier is *covariate mismatch*: the two sources measure different, only partially overlapping, covariates. We propose CALM (Calibrated ALignment under covariate Mismatch), which bypasses imputation by learning embeddings that map each source’s features into a common representation space. OS outcome models are transferred to the RCT embedding space and calibrated using trial data, preserving causal identification from randomization. Finite-sample risk bounds decompose into *alignment error*, *outcome-model complexity*, and *calibration complexity* terms, identifying when embedding alignment outperforms imputation. Under the calibration-based linear variant, the framework provides protection against negative transfer; the neural variant can be vulnerable under severe distributional shift. Under sparse linear models, the embedding approach strictly generalizes imputation. Simulations across 51 settings confirm that (i) calibration-based methods are equivalent for linear CATEs, and (ii) the neural embedding variant wins all 22 nonlinear-regime settings with large margins.

1 INTRODUCTION

Heterogeneous treatment effects (HTEs) are central to precision medicine: understanding how individual patient characteristics modulate treatment response enables clinicians to tailor interventions for maximal benefit [Kosorok and Laber, 2019]. Randomized controlled trials remain the gold

standard for causal inference, providing unconfounded treatment comparisons that support consistent estimation of the conditional average treatment effect,

$$\tau^r(\mathbf{x}) = \mathbb{E}[Y(1) - Y(-1) \mid \mathbf{X} = \mathbf{x}, S = r],$$

where $Y(a)$ denotes the potential outcome under treatment $a \in \{-1, 1\}$ and $S = r$ indicates the RCT population. In practice, however, most RCTs are powered for average effects rather than the fine-grained heterogeneity that guides individualized decisions [Wang et al., 2007, Kent et al., 2020]. At the same time, large-scale observational studies—electronic health records (EHRs), registries, and insurance claims—provide rich covariates and massive sample sizes, but are vulnerable to confounding.

This asymmetry motivates the integration of OS data to improve the precision of within-trial CATE estimation. Asiaee et al. [2023] formalize this $\mathcal{O} \rightarrow \mathcal{R}$ direction by introducing the *counterfactual mean outcome* (CMO) as the variance-minimizing augmentation function for pseudo-outcome regression, and propose R-OSCAR, a two-stage calibration procedure that learns outcome models from the OS, calibrates them to the RCT, and uses the calibrated predictions as an augmentation function. The key structural insight is that the OS enters only through the quality of the CMO estimate: better CMO estimation reduces both the irreducible variance and the estimation error of the CATE, while the causal identification remains anchored entirely in the randomized contrast.

The covariate mismatch barrier. A major obstacle to RCT–OS integration is that the covariates collected in trials and observational sources rarely align—a problem we call *covariate mismatch*. The RCT may contain behavioral or survey-based variables absent from the OS, while the OS may contain laboratory or utilization features not recorded in the trial [Rässler, 2002]. This differs fundamentally from *covariate shift* [Sugiyama and Kawanabe, 2012], where the same variables are observed but follow different distributions. Under mismatch, the outcome models trained on OS features cannot be directly evaluated on RCT units, breaking the core transfer step in data-borrowing methods. Indeed,

*Correspondence to: Amir Asiaee
<amir.asiaee@vumc.org>

Colnet et al. [2022] show that imputing covariates that were never measured in the trial cannot recover the required identification, even under perfectly specified linear models. (This identification limitation concerns transportability when key effect modifiers are absent from the trial; our use of imputation in MR-OSCAR serves only as augmentation for variance reduction, with causal identification anchored in RCT randomization.)

Partitioning covariates into shared ($\mathbf{Z} \in \mathbb{R}^{p_z}$), RCT-only ($\mathbf{U} \in \mathbb{R}^{p_u}$), and OS-only ($\mathbf{V} \in \mathbb{R}^{p_v}$) blocks (formalized in Section 3), a natural approach is to address covariate mismatch within the R-OSCAR framework by learning an imputation function $\hat{g} : \mathbb{R}^{p_z} \rightarrow \mathbb{R}^{p_v}$ that predicts \mathbf{V} from \mathbf{Z} in the OS, and then using \hat{g} to fill in the structurally missing \mathbf{V} block in the RCT. We call this the *mismatch-aware* extension, MR-OSCAR [Pal et al., 2026], which inherits R-OSCAR’s calibration-based negative-transfer protection and comes with finite-sample risk bounds that include an explicit *imputation error* term $L^2 r_{\text{im}}^2$, where L is a Lipschitz constant and r_{im}^2 is the oracle imputation risk (see Section 3.3).

Imputation is a harder problem than needed. The imputation approach requires reconstructing the entire \mathbf{V} vector in the RCT—a potentially high-dimensional regression problem whose difficulty scales with p_v and the complexity of $P(\mathbf{V} \mid \mathbf{Z})$. Yet, for the purpose of CATE estimation, all that is needed is a representation that is sufficient for (i) predicting outcomes and (ii) estimating discrepancy functions. When the outcome-relevant information in \mathbf{V} lies on a low-dimensional manifold, the imputation approach pays an unnecessarily high price by attempting to recover the full \mathbf{V} rather than its outcome-relevant projection.

Our contribution: embedding alignment. In this paper, we propose CALM, which replaces imputation with *representation alignment*. Instead of reconstructing missing covariates, we learn embedding functions $\phi^o : \mathbb{R}^{p_o} \rightarrow \mathbb{R}^d$ and $\phi^r : \mathbb{R}^{p_r} \rightarrow \mathbb{R}^d$ that map the heterogeneous feature spaces into a common d -dimensional representation space \mathcal{H} . Outcome models are trained in the OS embedding space and then transferred to the RCT embedding space, where they are calibrated and used for CATE estimation following the double-calibration pipeline of R-OSCAR. Crucially, OS data only inform the pseudo-outcome used to reduce variance of the CATE estimate (see Figure 1 for an overview); causal identification rests entirely on randomization within the trial and remains intact.

Our contributions are:

1. **Embedding-alignment framework.** We introduce CALM, which integrates representation learning into the R-OSCAR calibration pipeline, replacing imputation with learned embeddings. The framework inherits double-calibration-based negative-transfer protection.
2. **Finite-sample risk bounds.** We derive non-asymptotic bounds that decompose into alignment error and

outcome-model, calibration, and CATE-class complexity terms, making explicit when embedding outperforms imputation. Under linear Gaussian models, CALM strictly generalizes imputation-based approaches.

3. **Extensive experiments.** Linear and neural-network instantiations are validated across 51 simulation settings and an IHDP semi-synthetic benchmark.

2 RELATED WORK

CATE estimation uses meta-learners [Künzel et al., 2019, Kennedy, 2023, Nie and Wager, 2021], causal forests [Athey et al., 2019], Bayesian methods [Hahn et al., 2020], and representation-learning approaches [Johansson et al., 2016, Shalit et al., 2017, Yao et al., 2018, Shi et al., 2019, Hassani and Greiner, 2020]. Most RCT–OS integration work targets the $\mathcal{R} \rightarrow \mathcal{O}$ (generalizability) direction [Colnet et al., 2024, Degtiar and Rose, 2023, Dahabreh et al., 2020]; in the $\mathcal{O} \rightarrow \mathcal{R}$ direction, Cheng and Cai [2021] adaptively weight CATE estimates from both sources, Oberst et al. [2022] study optimal biased–unbiased combinations, Karlsson et al. [2025] provide worst-case guarantees, and the R-OSCAR framework of Asiaee et al. [2023] introduces a double-calibration procedure with non-asymptotic risk bounds; we extend it to the covariate-mismatch setting via two baselines (MR-OSCAR, SR-OSCAR) formalized in Section 3.3 and our main contribution CALM, which replaces imputation with representation alignment. In heterogeneous transfer learning, standard domain-adaptation methods [Ben-David et al., 2010, Ganin et al., 2016, Long et al., 2015, Pan and Yang, 2010, Weiss et al., 2016] assume shared features; cross-domain approaches use CCA variants [Hardoon et al., 2004, Andrew et al., 2013] or shared-private encoders [Bousmalis et al., 2016], and in the causal setting Bica and van der Schaar [2022] propose HTCE-learners, which require unconfoundedness in both domains, lack calibration-based negative-transfer protection, and provide no finite-sample guarantees. Sufficient dimension reduction [Cook, 2007, Li, 2018, Ma and Zhu, 2012, Ghosh et al., 2021] also targets outcome-relevant projections but does not address cross-dataset covariate mismatch. Bayesian borrowing via power priors [Ibrahim and Chen, 2000] and commensurate priors [Hobbs et al., 2011] discounts external data through a power parameter; our framework instead operates in a frequentist setting with calibration-based correction. Negative transfer is a well-documented risk [Rosenstein et al., 2005]; recent causal-inference work addresses it through optimal estimator combinations [Oberst et al., 2022], worst-case guarantees [Karlsson et al., 2025], and calibration [Asiaee et al., 2023], which CALM inherits, adding representation alignment.

3 PROBLEM SETUP AND BACKGROUND

3.1 NOTATION AND DATA STRUCTURE

We consider two data sources: a randomized controlled trial ($S = r$) and a large observational study ($S = o$). Let Y denote the outcome of interest, $A \in \{-1, 1\}$ the binary

treatment indicator, and $Y(a)$ the potential outcome under treatment a . We assume consistency: $Y = Y(A)$.

Each source observes a different subset of baseline covariates: the RCT records \mathbf{X}^r and the OS records \mathbf{X}^o . We denote the covariates measured in both sources by $\mathbf{Z} \in \mathbb{R}^{p_z}$ (the shared block), those exclusive to the RCT by $\mathbf{U} := \mathbf{X}^r \setminus \mathbf{Z} \in \mathbb{R}^{p_u}$, and those exclusive to the OS by $\mathbf{V} := \mathbf{X}^o \setminus \mathbf{Z} \in \mathbb{R}^{p_v}$, so that $\mathbf{X}^r = (\mathbf{U}, \mathbf{Z}) \in \mathbb{R}^{p_r}$ and $\mathbf{X}^o = (\mathbf{Z}, \mathbf{V}) \in \mathbb{R}^{p_o}$, where $p_r = p_u + p_z$ and $p_o = p_z + p_v$. We write $\mathbf{X} = (\mathbf{U}, \mathbf{Z}, \mathbf{V}) \in \mathbb{R}^p$ with $p = p_u + p_z + p_v$ for the complete covariate vector, and use lowercase $\mathbf{x}^r = (\mathbf{u}, \mathbf{z})$, $\mathbf{x}^o = (\mathbf{z}, \mathbf{v})$ for generic realizations.

The observed data are $\{(\mathbf{X}_i^r, A_i, Y_i)\}_{i=1}^{n^r}$ from the RCT and $\{(\mathbf{X}_j^o, A_j, Y_j)\}_{j=1}^{n^o}$ from the OS, with $n^r \ll n^o$ in the typical regime of interest. Let n_a^s denote the number of units in arm a under source s .

For each source $s \in \{r, o\}$ and arm $a \in \{-1, 1\}$, define the arm-specific conditional mean outcome

$$\mu_a^s(\mathbf{x}) = \mathbb{E}[Y \mid \mathbf{X}=\mathbf{x}, A=a, S=s],$$

and the RCT propensity score $\pi_a^r(\mathbf{x}^r) = \mathbb{P}(A = a \mid \mathbf{X}^r = \mathbf{x}^r, S = r)$.

Our inferential target is the CATE in the RCT population, marginalized over the unobserved \mathbf{V} :

$$\tau^r(\mathbf{x}^r) = \mathbb{E}[Y(1) - Y(-1) \mid \mathbf{X}^r = \mathbf{x}^r, S = r]. \quad (1)$$

3.2 THE CMO-AUGMENTED PSEUDO-OUTCOME FRAMEWORK

Following Asiaee et al. [2023], we construct pseudo-outcomes using an augmentation function $m : \mathbb{R}^{p_r} \rightarrow \mathbb{R}$:

$$\tau_m(\mathbf{X}^r, A, Y) = \frac{A(Y - m(\mathbf{X}^r))}{\pi_A^r(\mathbf{X}^r)}. \quad (2)$$

Under the standard RCT identification assumptions (SUTVA, ignorability, positivity), $\mathbb{E}[\tau_m \mid \mathbf{X}^r, S = r] = \tau^r(\mathbf{X}^r)$ for any m , so the pseudo-outcome is unbiased for the CATE. The CATE is then estimated by minimizing the empirical squared loss:

$$\hat{\tau}^r \in \arg \min_{f \in \mathcal{F}} \frac{1}{n^r} \sum_{i: S_i=r} (\tau_m(\mathbf{X}_i^r, A_i, Y_i) - f(\mathbf{X}_i^r))^2. \quad (3)$$

The central result of Asiaee et al. [2023] is that the variance of τ_m (and hence the efficiency of the CATE estimator) is minimized when m equals the *counterfactual mean outcome*:

$$\tilde{\mu}^r(\mathbf{x}^r) = \mathbb{E}\left[\sum_a \pi_{-a}^r(\mathbf{x}^r) \mu_a^r(\mathbf{X}) \mid \mathbf{X}^r = \mathbf{x}^r, S = r\right]. \quad (4)$$

The quality of the augmentation function directly governs the CATE estimation risk. Specifically, the prediction risk decomposes as [Asiaee et al., 2023]:

$$R_m(\hat{\tau}) = \underbrace{\mathbb{E}_{\mathbf{X}^r} [\text{Var}(\tau_m \mid \mathbf{X}^r)]}_{\text{irreducible error}} + \underbrace{\Delta_2^2(\hat{\tau}, \tau^r)}_{\text{CATE estimation error}}, \quad (5)$$

where $\Delta_2^2(f, g) = \mathbb{E}[(f(\mathbf{X}^r) - g(\mathbf{X}^r))^2 \mid S = r]$. Both terms are controlled by $\Delta_2^2(m, \tilde{\mu}^r)$, the accuracy of the CMO estimate: the irreducible error satisfies $\mathbb{E}[\text{Var}(\tau_m \mid \mathbf{X}^r)] - \mathbb{E}[\text{Var}(\tau_{\tilde{\mu}^r} \mid \mathbf{X}^r)] \asymp \Delta_2^2(m, \tilde{\mu}^r)$, and the estimation error bound scales multiplicatively with $1 + \Delta_2(m, \tilde{\mu}^r)$ times the Rademacher complexity $\mathcal{R}_{n^r}(\mathcal{F})$ of the CATE function class.

This motivates borrowing from the OS to obtain a better estimate of the CMO.

3.3 THE R-OSCAR PIPELINE AND IMPUTATION-BASED BASELINES

We first review the R-OSCAR pipeline [Asiaee et al., 2023] and then introduce two natural baselines for extending it to the covariate mismatch setting.

R-OSCAR without covariate mismatch. When there is no covariate mismatch (i.e., $p_u = p_v = 0$), the R-OSCAR pipeline operates as follows:

1. **OS outcome model:** For each arm a , learn $\hat{\mu}_a^o(\mathbf{x})$ from OS data.
2. **Outcome calibration:** Estimate a discrepancy function $\hat{\delta}_a^t(\mathbf{x})$ from RCT data so that $\hat{\mu}_a^o(\mathbf{x}) + \hat{\delta}_a^t(\mathbf{x}) \approx \mu_a^r(\mathbf{x})$. The calibrated CMO is $\hat{m}(\mathbf{x}) = \sum_a \pi_{-a}^r(\mathbf{x}) [\hat{\mu}_a^o(\mathbf{x}) + \hat{\delta}_a^t(\mathbf{x})]$.
3. **CATE calibration:** Using \hat{m} as the augmentation function, form pseudo-outcomes and estimate a CATE correction $\hat{\delta}(\mathbf{x})$, yielding $\hat{\tau}_{\text{R-OSCAR}}(\mathbf{x}) = \sum_a a [\hat{\mu}_a^o(\mathbf{x}) + \hat{\delta}_a^t(\mathbf{x})] + \hat{\delta}(\mathbf{x})$.

The two-stage design decouples nuisance estimation from CATE estimation: misspecification in outcome models affects only the augmentation quality (variance), while CATE consistency depends only on correct specification of the CATE discrepancy $\hat{\delta}$.

Under covariate mismatch, Pal et al. [2026] propose an imputation-based extension, MR-OSCAR, which adds a preliminary step: learn $\hat{g} : \mathbb{R}^{p_z} \rightarrow \mathbb{R}^{p_v}$ in the OS, set $\hat{\mathbf{V}}_i = \hat{g}(\mathbf{Z}_i)$ for RCT units, and then run R-OSCAR using $(\mathbf{X}^r, \hat{\mathbf{V}})$ in the RCT. An even simpler baseline, SR-OSCAR [Pal et al., 2026], forgoes imputation entirely and applies R-OSCAR using only the shared covariates \mathbf{Z} . The finite-sample risk bound for MR-OSCAR [Pal et al., 2026] is:

$$\begin{aligned} \Delta_2^2(\hat{\tau}_{\text{MR-OSCAR}}, \tau^r) &\lesssim \Delta_2^2(\mathcal{F}, \tau^r) + L^2 r_{\text{im}}^2 + \mathfrak{R}_{n^r}^2(\mathcal{F}) \\ &+ \sum_a (\mathfrak{R}_{n^o}^2(\mathcal{M}_a^{\text{o:im}}) + \mathfrak{R}_{n^r}^2(\mathcal{D}_a^{\text{im}})) + \mathfrak{R}_{n^o}^2(\mathcal{G}), \end{aligned} \quad (6)$$

where $r_{\text{im}}^2 = \mathbb{E}[\|\mathbf{V} - g^*(\mathbf{Z})\|^2 \mid S = o]$ is the oracle imputation risk and L is the Lipschitz constant of the outcome models in \mathbf{V} .

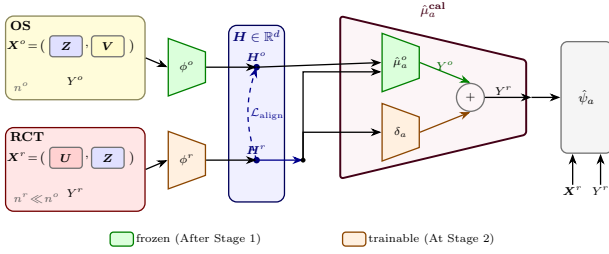


Figure 1: How OS data inform pseudo-outcome construction in CALM. OS and RCT data pass through source-specific encoders ϕ^o (frozen after Stage 1) and ϕ^r (trainable at Stage 2) into a shared embedding space $\mathbf{H} \in \mathbb{R}^d$. The calibrated outcome model $\hat{\mu}_a^r = \hat{\mu}_a^o + \delta_a^t$ combines the frozen OS outcome head with a learnable shift. Pseudo-outcomes $\hat{\psi}_a^r$ are then constructed from these calibrated predictions together with the RCT covariates and outcomes. The calibrated model $\hat{\mu}_a^r$ is also used in the subsequent CATE calibration stage (Stage 4 of Algorithm 1).

4 CALM: EMBEDDING-ALIGNED CATE ESTIMATION

We now present CALM, our framework for addressing covariate mismatch through representation alignment rather than imputation.

4.1 CORE IDEA: FROM IMPUTATION TO ALIGNMENT

The key observation is that the R-OSCAR pipeline requires not the raw covariates but rather *a common representation* in which (i) outcome models can be meaningfully evaluated for both OS and RCT units, and (ii) discrepancy functions can be estimated. Imputation achieves this by reconstructing the missing \mathbf{V} block, but this is an intermediate step that solves a harder problem than necessary.

CALM instead learns embedding functions $\phi^o : \mathbb{R}^{p_o} \rightarrow \mathbb{R}^d$ (OS encoder) and $\phi^r : \mathbb{R}^{p_r} \rightarrow \mathbb{R}^d$ (RCT encoder) that map each source’s full feature vector into a shared d -dimensional space \mathcal{H} . The OS outcome model is trained on the OS embeddings $\hat{\mu}_a^o(\phi^o(\mathbf{X}^o))$ and then evaluated on the RCT embeddings $\hat{\mu}_a^o(\phi^r(\mathbf{X}^r))$ during calibration. If units with similar \mathbf{Z} produce similar embeddings, the OS outcome model provides a useful initial prediction when applied to RCT embeddings, and the calibration step corrects for residual discrepancy.

4.2 ASSUMPTIONS

We maintain the standard causal identification assumption for the RCT.

Assumption 1 (Internal validity of the RCT). SUTVA holds; $(Y(1), Y(-1)) \perp\!\!\!\perp A \mid (\mathbf{X}^r, S = r)$; and there exists $\rho > 0$ such that $\rho \leq \pi_a^r(\mathbf{X}^r) \leq 1 - \rho$ almost surely for each a .

Rather than requiring full distributional transportability of $\mathbf{V} \mid \mathbf{Z}$ as in MR-OSCAR, we introduce an embedding-level assumption.

Assumption 2 (Outcome-sufficient embedding). For fixed encoders ϕ^o and ϕ^r , the per-arm outcome means in each

source are well-approximated by functions of the embeddings: there exist functions $\tilde{\mu}_a^s : \mathbb{R}^d \rightarrow \mathbb{R}$ in function class \mathcal{M}_a^s such that

$$\mathbb{E}[(\mu_a^s(\mathbf{X}^s) - \tilde{\mu}_a^s(\phi^s(\mathbf{X}^s)))^2 \mid S = s] \leq \epsilon_{\text{suff}}^2,$$

for $s \in \{o, r\}$ and arm a , where ϵ_{suff}^2 is the *sufficiency gap*.

This is weaker than requiring the embedding to be a sufficient statistic for the outcome: we allow an approximation error ϵ_{suff}^2 that vanishes as d grows.

Assumption 3 (Outcome shift in embedding space). For each arm a , there exists a discrepancy function $\delta_a : \mathbb{R}^d \rightarrow \mathbb{R}$ in a function class \mathcal{D}_a of controlled complexity such that

$$\tilde{\mu}_a^r(\mathbf{h}) = \tilde{\mu}_a^o(\mathbf{h}) + \delta_a(\mathbf{h}),$$

where $\tilde{\mu}_a^s$ are the population-level outcome functions operating on the embedding $\mathbf{h} \in \mathbb{R}^d$.

This is the direct analogue of the outcome-shift assumption in the original R-OSCAR framework [Asiaee et al., 2023], but stated in the embedding space rather than the covariate space. It allows outcome means and CATEs to differ arbitrarily between the RCT and OS; the discrepancy is modeled and estimated from RCT data.

Assumption 4 (Alignment quality). The alignment error between the two encoders, measured on the RCT distribution, is bounded:

$$r_\phi^2 := \mathbb{E}[\|\phi^o(\mathbf{X}^{o,*}) - \phi^r(\mathbf{X}^r)\|^2 \mid S = r] < \infty,$$

where $\mathbf{X}^{o,*} = (\mathbf{Z}, \mathbf{V}^*)$ with \mathbf{V}^* denoting the (unobserved) value that \mathbf{V} would take for an RCT unit. Furthermore, the outcome model $\tilde{\mu}_a^o$ is L_μ -Lipschitz in its argument and the discrepancy δ_a is L_δ -Lipschitz.

In practice, r_ϕ^2 is not directly computable since \mathbf{V} is unobserved in the RCT. Instead, it is controlled indirectly through the alignment objective used during training (see Section 4.4). The Lipschitz conditions ensure that small alignment errors translate to small prediction errors.

4.3 THE CALM ALGORITHM

The CALM procedure consists of four stages.

Stage 1: OS outcome model in embedding space. Train the OS encoder ϕ^o and per-arm outcome heads $\hat{\mu}_a^o : \mathbb{R}^d \rightarrow \mathbb{R}$ jointly on OS data:

$$\begin{aligned} (\hat{\phi}^o, \hat{\mu}_{-1}^o, \hat{\mu}_{+1}^o) \in \arg \min_{\phi^o, \mu_a} \sum_{a \in \{-1, 1\}} \frac{1}{n_a^o} \\ \times \sum_{i: A_i = a, S_i = o} (Y_i - \mu_a(\phi^o(\mathbf{X}_i^o)))^2 + \mathcal{P}_{\text{OS}}, \quad (7) \end{aligned}$$

where \mathcal{P}_{OS} is a regularization penalty (e.g., ℓ_1 , weight decay, or dropout).

Stage 2: RCT encoder alignment and outcome calibration. Fix $\hat{\phi}^o$ and $\hat{\mu}_a^o$ from Stage 1. Learn the RCT encoder

Algorithm 1 CALM: Calibrated Alignment under Covariate Mismatch

Require: OS data $\{(\mathbf{X}_j^o, A_j, Y_j)\}_{j=1}^{n^o}$; RCT data $\{(\mathbf{X}_i^r, A_i, Y_i)\}_{i=1}^{n^r}$; embedding dimension d ; alignment weight λ .

- 1: **Stage 1:** Train OS encoder $\hat{\phi}^o$ and outcome heads $\hat{\mu}_a^o$ via (7).
 - 2: **Stage 2:** Learn RCT encoder $\hat{\phi}^r$ and discrepancies $\hat{\delta}_a^t$ via (8).
 - 3: **Stage 3:** Compute calibrated CMO \hat{m} via (10); form pseudo-outcomes $\hat{\psi}_i^r$.
 - 4: **Stage 4:** Estimate CATE correction $\hat{\delta}$ via (11).
 - 5: **return** $\hat{\tau}_{\text{CALM}}(\mathbf{x}^r) = \tilde{\tau}(\mathbf{x}^r) + \hat{\delta}(\mathbf{x}^r)$
-

$\hat{\phi}^r$ and arm-specific discrepancy functions $\hat{\delta}_a^t : \mathbb{R}^d \rightarrow \mathbb{R}$ by minimizing a calibration loss with an alignment penalty:

$$(\hat{\phi}^r, \hat{\delta}_a^t) \in \arg \min_{\phi^r, d_a} \sum_a \frac{1}{n_a^r} \sum_{i: A_i=a, S_i=r} \left(Y_i - \hat{\mu}_a^o(\phi^r(\mathbf{X}_i^r)) - d_a(\phi^r(\mathbf{X}_i^r)) \right)^2 + \mathcal{P}_{\text{cal}}(d_a) + \lambda \mathcal{L}_{\text{align}}(\hat{\phi}^o, \phi^r). \quad (8)$$

Here, \mathcal{P}_{cal} controls the complexity of the discrepancy (encouraging borrowing from the OS by shrinking d_a toward zero), and $\mathcal{L}_{\text{align}}$ is an alignment loss (see Section 4.4).

Stage 3: Calibrated CMO and pseudo-outcome construction. Compute the calibrated arm-specific predictions and the calibrated CMO for RCT units:

$$\hat{\mu}_a^{\text{cal}}(\mathbf{x}^r) = \hat{\mu}_a^o(\hat{\phi}^r(\mathbf{x}^r)) + \hat{\delta}_a^t(\hat{\phi}^r(\mathbf{x}^r)), \quad (9)$$

$$\hat{m}(\mathbf{x}^r) = \sum_a \pi_{-a}^r(\mathbf{x}^r) \hat{\mu}_a^{\text{cal}}(\mathbf{x}^r). \quad (10)$$

Form **pseudo-outcomes** $\hat{\psi}_i^r = A_i(Y_i - \hat{m}(\mathbf{X}_i^r))/\pi_{A_i}^r(\mathbf{X}_i^r)$ for each RCT unit.

Stage 4: CATE correction. The preliminary CATE is $\tilde{\tau}(\mathbf{x}^r) = \sum_a a \hat{\mu}_a^{\text{cal}}(\mathbf{x}^r)$. Estimate a CATE correction $\hat{\delta} : \mathbb{R}^{p_r} \rightarrow \mathbb{R}$ using RCT data:

$$\hat{\delta} \in \arg \min_{d \in \mathcal{D}} \frac{1}{n^r} \sum_{i: S_i=r} (\hat{\psi}_i^r - \tilde{\tau}(\mathbf{X}_i^r) - d(\mathbf{X}_i^r))^2 + \mathcal{P}_{\tau}(d). \quad (11)$$

The final CALM estimator is:

$$\hat{\tau}_{\text{CALM}}(\mathbf{x}^r) = \tilde{\tau}(\mathbf{x}^r) + \hat{\delta}(\mathbf{x}^r). \quad (12)$$

Note that the CATE calibration (Stage 4) operates on the *original* RCT covariates \mathbf{X}^r , not on the embedding. This ensures that the final CATE estimate is interpretable in terms of the original covariates; causal identification is preserved by the unbiasedness of the pseudo-outcomes under RCT randomization (Assumption 1).

The full procedure is summarized in Algorithm 1.

4.4 ALIGNMENT OBJECTIVES

The alignment loss $\mathcal{L}_{\text{align}}$ encourages the two encoders to produce compatible representations. Since \mathbf{V} is unobserved in the RCT and \mathbf{U} in the OS, we cannot directly minimize

$\|\phi^o(\mathbf{X}^o) - \phi^r(\mathbf{X}^r)\|^2$ on paired units; instead, alignment is achieved through the shared covariates \mathbf{Z} . We consider two approaches. *Distribution-matching alignment* (MMD) uses the kernel maximum mean discrepancy [Gretton et al., 2012]:

$$\mathcal{L}_{\text{MMD}} = \left\| \frac{1}{n^o} \sum_{j \in \text{OS}} k(\hat{\phi}^o(\mathbf{X}_j^o), \cdot) - \frac{1}{n^r} \sum_{i \in \text{RCT}} k(\phi^r(\mathbf{X}_i^r), \cdot) \right\|_{\mathcal{H}_k}^2, \quad (13)$$

which encourages the marginal embedding distributions to match (see Appendix B for the expanded objective and additional alignment variants). *Z-conditioned contrastive alignment* matches units with similar shared covariates:

$$\mathcal{L}_{\text{contr}} = \frac{1}{n^r} \sum_{i \in \text{RCT}} \frac{1}{|N_i|} \sum_{j \in N_i} \|\hat{\phi}^o(\mathbf{X}_j^o) - \phi^r(\mathbf{X}_i^r)\|^2, \quad (14)$$

where $N_i = \{j \in \text{OS} : \|\mathbf{Z}_j - \mathbf{Z}_i\| \leq \varepsilon\}$. Adversarial alignment [Ganin et al., 2016] is also applicable (Appendix B).

5 THEORETICAL ANALYSIS

We now derive finite-sample risk bounds for CALM and compare them to the MR-OSCAR bounds. All proofs are deferred to Appendix A.

5.1 RISK BOUND FOR CALM

Theorem 1 (Risk bound for CALM). *Suppose Assumptions 1–4 hold, and all nuisance estimators are obtained via penalized empirical risk minimizer with sample splitting or cross-fitting across stages. Let \mathcal{D} be the function class for the CATE correction in Stage 4 (Algorithm 1), and let $\mathcal{F} = \{\tilde{\tau} + d : d \in \mathcal{D}\}$ be the induced class for the final CATE estimator on \mathbf{X}^r . Let \mathcal{M}_a^o be the class for OS outcome models on \mathbb{R}^d and \mathcal{D}_a the class for arm-specific discrepancy on \mathbb{R}^d . Then there exists a constant $C > 0$ such that, with probability at least $1 - \gamma$:*

$$\begin{aligned} \Delta_2^2(\hat{\tau}_{\text{CALM}}, \tau^r) &\leq \Delta_2^2(\mathcal{F}, \tau^r) + C \frac{\log(1/\gamma)}{n^r} \\ &+ C \left[\underbrace{\epsilon_{\text{suff}}^2}_{\text{suff.}} + \underbrace{(L_\mu + L_\delta)^2 r_\phi^2}_{\text{align.}} + \underbrace{\sum_a \mathfrak{R}_{n^o}^2(\mathcal{M}_a^o)}_{\text{OS}} \right. \\ &\left. + \underbrace{\sum_a \mathfrak{R}_{n^r}^2(\mathcal{D}_a)}_{\text{calib.}} + \underbrace{\mathfrak{R}_{n^r}^2(\mathcal{F})}_{\text{CATE}} \right]. \end{aligned} \quad (15)$$

Proof sketch. We decompose the augmentation error into estimation (I), alignment (II), sufficiency (III), and marginalization (IV) terms, bound each using Lipschitz continuity (Assumption 4) and empirical process arguments, and combine via the CMO calibration framework of Asiaee et al. [2023]. The full proof is in Appendix A. \square

5.2 COMPARISON WITH MR-OSCAR AND SR-OSCAR

Corollary 2 (When CALM improves over MR-OSCAR). *Assume both estimators use function classes of comparable*

complexity for calibration [see Pal et al., 2026, for the MR-OSCAR bound]. Then CALM yields a tighter bound than MR-OSCAR whenever

$$\begin{aligned} \epsilon_{\text{sufl}}^2 + (L_\mu + L_\delta)^2 r_\phi^2 + \sum_a \mathfrak{R}_{n^o}^2(\mathcal{M}_a^o) \\ < L^2 r_{\text{im}}^2 + \sum_a \mathfrak{R}_{n^o}^2(\mathcal{M}_a^{o,\text{im}}) + \mathfrak{R}_{n^o}^2(\mathcal{G}). \end{aligned} \quad (16)$$

This holds when:

1. $d \ll p_o$, so outcome models in \mathbb{R}^d have lower Rademacher complexity than those in \mathbb{R}^{p_o} ;
2. \mathbf{V} is hard to reconstruct but easy to summarize: $r_\phi^2 \ll r_{\text{im}}^2$ because the outcome-relevant information in \mathbf{V} lies on a low-dimensional manifold;
3. The sufficiency gap ϵ_{sufl}^2 is small, i.e., the embedding captures most outcome-relevant variation.

The trade-off is clear: CALM gains from dimensionality reduction but pays for information loss (ϵ_{sufl}^2) and alignment imperfection (r_ϕ^2), while MR-OSCAR avoids information loss but pays the full imputation cost (r_{im}^2 in \mathbb{R}^{p_v}).

5.3 NEGATIVE-TRANSFER PROTECTION

Proposition 3 (Safe borrowing). *Under the conditions of Theorem 1, the pseudo-outcome $\hat{\psi}^r$ remains unbiased for $\tau^r(\mathbf{X}^r)$ regardless of augmentation quality (Eq. 2). When alignment error $(L_\mu + L_\delta)^2 r_\phi^2$ is large, Stage 4 compensates by learning a correction $\hat{\delta}(\mathbf{X}^r)$ that captures the full CATE from RCT data alone; consistency is preserved but variance reduction from OS borrowing is lost. This protection is complete for CALM-Lin; for CALM-NN under severe distributional shift, the learned encoder may distort the embedding space.*

5.4 SPECIALIZATION TO SPARSE LINEAR MODELS

To build further intuition, we specialize CALM to a linear setting. Let the encoders be linear projections $\phi^o(\mathbf{X}^o) = \mathbf{W}^o(\mathbf{X}^o)^\top$ and $\phi^r(\mathbf{X}^r) = \mathbf{W}^r(\mathbf{X}^r)^\top$, where $\mathbf{W}^o \in \mathbb{R}^{d \times p_o}$ and $\mathbf{W}^r \in \mathbb{R}^{d \times p_r}$. Let the outcome model be linear in the embedding: $\tilde{\mu}_a^o(\mathbf{h}) = \beta_a^\top \mathbf{h}$.

Proposition 4 (Linear embedding and imputation). *Under Gaussian covariates with $\mathbf{V} = \mathbf{\Lambda}\mathbf{Z} + \epsilon_V$ and $\mathbf{U} \perp\!\!\!\perp \mathbf{V} \mid \mathbf{Z}$, the optimal linear embedding that minimizes alignment error subject to preserving outcome-relevant information satisfies*

$$\mathbf{W}_{\text{opt}}^r = \mathbf{W}^o \begin{pmatrix} \mathbf{0}_{p_z \times p_u} & \mathbf{I}_{p_z} \\ \mathbf{0}_{p_v \times p_u} & \mathbf{\Lambda} \end{pmatrix},$$

which is equivalent to imputing $\hat{\mathbf{V}} = \mathbf{\Lambda}\mathbf{Z}$ and then projecting $(\mathbf{Z}, \hat{\mathbf{V}})$ through \mathbf{W}^o .

This reveals that, in the linear case, the alignment-based approach with a d -dimensional embedding is equivalent to imputation followed by dimensionality reduction to \mathbb{R}^d . The embedding approach thus *strictly generalizes* MR-OSCAR:

when $d = p_o$, it recovers MR-OSCAR; when $d < p_o$, it achieves additional variance reduction through projection.

Corollary 5 (Linear CALM risk bound). *Under the conditions of Proposition 4, if the outcome model has sparsity s in the embedding space and the discrepancy has sparsity s_δ , then*

$$\begin{aligned} \Delta_2^2(\hat{\tau}_{\text{CALM}}, \tau^r) &\lesssim \underbrace{\Delta_2^2(\mathcal{F}, \tau^r)}_{\text{approx.}} + \underbrace{L_\mu^2 \text{tr}(\Sigma_{\mathbf{V}|\mathbf{Z}})}_{\text{irred. noise}} \\ &+ \underbrace{\frac{s \log d}{n^o}}_{\text{OS}} + \underbrace{\frac{s_\delta \log d}{n^r}}_{\text{calib.}} + \underbrace{\frac{s_\tau \log p_r}{n^r}}_{\text{CATE}}, \end{aligned}$$

where s_τ is the sparsity of the CATE. Compared to MR-OSCAR, the outcome model and calibration complexities scale with $\log d$ instead of $\log p_o$, yielding strictly tighter rates when $d \ll p_o$.

6 PRACTICAL IMPLEMENTATION

In the linear instantiation (CALM-Lin), all components reduce to penalized regressions: Stage 1 fits a reduced-rank regression (or LASSO in a PCA-reduced space) of Y on \mathbf{X}^o in the OS; Stage 2 constructs $\mathbf{W}^r = \mathbf{W}^o \begin{pmatrix} \mathbf{I}_{p_z} \\ \hat{\mathbf{\Lambda}} \end{pmatrix}$, where $\hat{\mathbf{\Lambda}}$ is a ridge/LASSO estimate of $\mathbb{E}[\mathbf{V} \mid \mathbf{Z}]$, and calibrates via LASSO on \mathbf{X}^r ; Stages 3–4 follow the standard R-OSCAR pipeline. In the neural instantiation (CALM-NN), the encoders ϕ^o and ϕ^r are MLPs with separate parameters and per-arm outcome heads; we recommend the \mathbf{Z} -conditioned contrastive loss (14) for small-to-moderate n^r and MMD (13) for larger samples. Stage 1 trains on OS data alone, Stage 2 jointly optimizes ϕ^r and $\hat{\delta}_a^t$ with the alignment penalty (optionally initializing ϕ^r from ϕ^o restricted to shared features), Stage 4 uses LASSO on \mathbf{X}^r for interpretability, and all nuisance estimates are cross-fitted over K RCT folds. The embedding dimension d controls the bias–variance trade-off: for CALM-Lin, d is set via cross-validated OS prediction error; for CALM-NN, d is a bottleneck hyperparameter selected by cross-validated CATE calibration error on the RCT.

7 EXPERIMENTS

We validate CALM through simulations designed to test the predictions of Section 5.

7.1 SIMULATION DESIGN

Data-generating process. We generate paired OS and RCT datasets as follows. Let $p_z = 30$, $p_u = 10$, $p_v = 20$, and $d_{\text{true}} = 5$ denote the intrinsic dimension of the outcome-relevant signal. Shared covariates are drawn as $\mathbf{Z} \sim \mathcal{N}(\mathbf{0}, \Sigma_{\mathbf{Z}\mathbf{Z}})$ with AR(1) correlation ($\rho = 0.5$); (i) OS-only covariates $\mathbf{V} = \mathbf{\Lambda}_{\mathbf{V}\mathbf{Z}}\mathbf{Z} + \epsilon_V$, $\epsilon_V \sim \mathcal{N}(\mathbf{0}, \sigma_V^2 \mathbf{I})$, and (ii) RCT-only covariates $\mathbf{U} = \mathbf{\Lambda}_{\mathbf{U}\mathbf{Z}}\mathbf{Z} + \epsilon_U$, $\epsilon_U \sim \mathcal{N}(\mathbf{0}, \sigma_U^2 \mathbf{I})$, are generated conditionally on \mathbf{Z} . Outcomes follow $Y^s(a) = f_a(\mathbf{P}^s \mathbf{X}^\top) + \delta_a^s(\mathbf{Z}) + \epsilon$, where \mathbf{P}^s projects to a d_{true} -dimensional subspace, f_a is a nonlinear function (with linear and sinusoidal variants), and δ_a^s

captures population-specific shifts. Treatment assignment in the OS uses a logistic model on 10 covariates; the RCT uses $\pi_{+1}^r = 0.5$.

Factors varied. Each experiment varies one factor while holding others at default values ($n^r = 500$, $\sigma_V^2 = 1.0$, $d_{\text{true}} = 5$, linear outcome, shift magnitude 0.5). The six factors are: imputation difficulty, $\sigma_V^2 \in \{0.1, 0.25, 0.5, 1.0, 2.0\}$ (higher σ_V^2 makes \mathbf{V} harder to predict from \mathbf{Z}); intrinsic dimension, $d_{\text{true}} \in \{2, 3, 5, 10, 15, 20\}$; RCT sample size, $n^r \in \{100, 250, 500, 1,000, 2,000\}$ with $n^o = 10,000$ fixed; outcome nonlinearity (linear, quadratic, sinusoidal); outcome shift magnitude, $\|\delta_a^r - \delta_a^o\| \in \{0, 0.25, 0.5, 1.0, 2.0, 5.0\}$; and shared covariate proportion, $p_z/(p_z + p_v) \in \{0.3, 0.5, 0.7, 0.9\}$.

7.2 METHODS UNDER COMPARISON

We compare eight methods: **Naive**, RCT-only CATE estimation with no augmentation ($m = 0$); **RACER**, RCT-only augmentation using outcome models fitted on \mathbf{X}^r in the RCT; **SR-OSCAR** [Pal et al., 2026], which borrows from OS using only shared covariates \mathbf{Z} (Section 3.3); **MR-OSCAR** [Pal et al., 2026], imputation-based borrowing (Section 3.3); **CALM-Lin**, the linear embedding version of CALM; **CALM-NN**, the neural network version of CALM (residual MLP encoders with an alignment loss); and **HTCE-T** and **HTCE-DR**, the transfer T-learner and DR-learner of Bica and van der Schaar [2022], respectively. For HTCE-T and HTCE-DR, we use the shared/private encoder architectures of Bica and van der Schaar [2022] and evaluate by cross-fitting predictions over RCT folds to avoid outcome leakage.

7.3 EVALUATION METRICS

We report the RMSE of CATE, $[(1/n^r) \sum_{i:S_i=r} (\hat{\tau}(\mathbf{X}_i^r) - \tau^r(\mathbf{X}_i^r))^2]^{1/2}$, averaged over 20 replicates (50 for the IHDP benchmark; Appendix C).

7.4 RESULTS: LINEAR CATE REGIME

All numbers below are mean RMSE over 20 replicates. The baseline regime comprises 29 settings in which the CATE is linear in the target covariates and a single mismatch factor is varied at a time. Across these 29 settings, the lowest mean RMSE is achieved by RACER in 11, CALM-Lin in 9, MR-OSCAR in 6, SR-OSCAR in 2, and HTCE-T in 1. All four calibration-based methods (RACER, SR-OSCAR, MR-OSCAR, CALM-Lin) are effectively indistinguishable in this regime: pairwise differences in mean RMSE are below 10^{-3} , and which method achieves the argmin depends on the factor varied. Table 1 reports representative values.

Imputation difficulty (Figure 2a). As σ_V^2 increases, all calibration-based methods degrade together. The argmin shifts with the noise level: RACER is best at $\sigma_V^2 \in \{0.1, 0.5, 2.0\}$ (RMSE 0.76, 0.91, and 1.45), CALM-Lin at $\sigma_V^2 = 0.25$ (0.83), and MR-OSCAR at $\sigma_V^2 = 1.0$ (1.03).

Table 1: Mean RMSE across imputation difficulty (σ_V^2 , linear outcome) and outcome nonlinearity ($\sigma_V^2 = 1.0$), averaged over 20 replicates. **Bold**: lowest per column.

Method	Imputation difficulty (σ_V^2)				Outcome	
	0.1	0.5	1.0	2.0	Quad.	Sin.
Naive	1.16	1.22	1.30	1.65	1.70	1.29
Calib. group [†]	0.76	0.91	1.03	1.45	1.45	1.06
CALM-NN	0.88	1.02	1.18	1.59	1.54	1.15
HTCE-T	1.15	1.28	1.45	1.93	1.81	1.43
HTCE-DR	1.17	1.36	1.48	1.98	1.92	1.50

[†]RACER, SR-OSCAR, MR-OSCAR, CALM-Lin: single representative; pairwise $\Delta\text{RMSE} < 10^{-3}$.

CALM-NN is consistently above the calibration-based methods in this linear-CATE setting.

Intrinsic dimension and shared proportion (Appendix C).

No single method dominates as d_{true} varies; the winner alternates among RACER ($d_{\text{true}} \in \{2, 15\}$), SR-OSCAR (10 and 20), MR-OSCAR (3), and CALM-Lin (5), with small gaps throughout. Similarly, as the shared covariate proportion increases, all methods improve and the identity of the best calibration-based method shifts: CALM-Lin at low and moderate overlap (0.3 and 0.5), MR-OSCAR at intermediate overlap (0.7), and RACER at high overlap (0.9).

RCT sample size (Appendix C). At $n^r = 100$ (baseline linear-CATE regime), HTCE-T yields the lowest RMSE (2.84), while the OS-borrowing calibration variants (SR-OSCAR, MR-OSCAR, CALM-Lin) can be unstable. For $n^r \geq 250$ the calibration-based methods converge; at $n^r = 2,000$, RACER, SR-OSCAR, MR-OSCAR, and CALM-Lin all achieve RMSE ≈ 0.53 .

Outcome nonlinearity and negative transfer (Figures 5, 7 in Appendix C).

Under outcome nonlinearity, RACER is best for linear outcomes (RMSE 1.15), CALM-Lin for quadratic (1.45), and MR-OSCAR for sinusoidal (1.06); CALM-NN does not improve over the strongest linear baselines here. Under increasing outcome shift, calibration-based methods remain stable (e.g., RMSE ≈ 1.11 for CALM-Lin at shift 5.0), whereas Naive inflates to 3.84 and HTCE-T to 3.32. CALM-NN is less robust at extreme shift (RMSE 2.25 at shift 5.0), consistent with the limitation that the alignment objective can distort the learned representation when the domain gap is large.

7.5 RESULTS: NONLINEAR-CATE REGIME

We next consider a regime in which the CATE is nonlinear in the target covariates. We modify the DGP so that the outcome-relevant signal is mediated entirely by \mathbf{V} through shared latent factors: \mathbf{U} and \mathbf{V} share a 5-dimensional latent factor \mathbf{H} (scale 2.0 in both measurement models, $\sigma_U^2 = \sigma_V^2 = 0.1$), and the outcome depends only on \mathbf{V} (signal weights $w_Z = w_U = 0$, $w_V = 2$). The CATE takes a nonlinear sinusoidal form with frequency parameter ω , so that $\tau^r(\mathbf{X}^r)$ is nonlinear after marginalization over \mathbf{V} . This regime, comprising 22 settings across the sweeps described below, is not included in the baseline grid. CALM-NN attains the lowest mean RMSE in all 22 settings, with margins

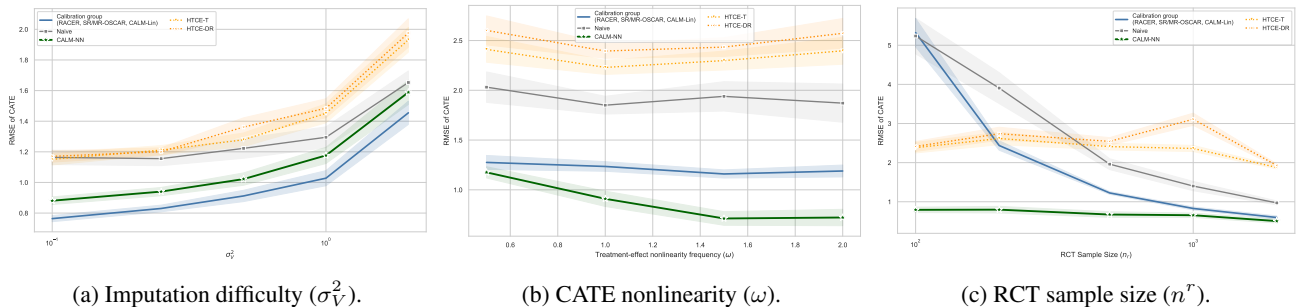


Figure 2: RMSE of CATE estimation across three experimental sweeps. Mean over 20 replicates. In all panels, the blue band groups four calibration-based methods (RACER, SR-OSCAR, MR-OSCAR, CALM-Lin) whose RMSEs are nearly identical; the band spans their min–max envelopes (mean \pm SE). Individual lines show the remaining methods. **(a)** $n^r = 500$, $n^o = 10,000$, $d_{\text{true}} = 5$, linear outcome. **(b)** Shared-latent DGP where \mathbf{X}^r carries information about \mathbf{V} beyond \mathbf{Z} ; CALM-NN separates from the calibration group as ω increases. **(c)** Nonlinear-CATE regime: CALM-NN maintains RMSE below 0.8 even at $n^r = 100$, where calibration-based methods exceed 5.3.

ranging from 0.09 to 4.53.

Treatment-effect frequency (Figure 2b). Across $\omega \in \{0.5, 1.0, 1.5, 2.0\}$, CALM-NN attains the lowest RMSE in all four settings. At $\omega = 1.5$, CALM-NN achieves RMSE 0.71 compared with 1.16 for CALM-Lin; at $\omega = 2.0$, RMSE is 0.72 versus 1.19 for the best calibration-based method, a 39% reduction. This confirms the regime predicted by Corollary 2: when outcome-relevant information is low-dimensional and the CATE is nonlinear, learned embeddings outperform imputation-based approaches.

Robustness to signal routing and CATE functional form (Appendix C). To test whether the advantage depends on the outcome signal being routed entirely through unobserved covariates \mathbf{V} , we vary the shared-covariate signal weight $w_Z \in \{0, 0.5, 1.0, 1.5, 2.0\}$ while holding $w_V = 2$ and $\omega = 1.5$. CALM-NN wins all 5 settings with margins of 0.45–0.59 over calibration-based methods, and the advantage does not diminish as w_Z increases (RMSE 0.62 vs. 1.12 at $w_Z = 2$). This indicates that the gain stems from the ability to model nonlinear CATEs, not from exploiting \mathbf{V} -specific information inaccessible to imputation-based approaches. The advantage also generalizes across CATE functional forms (absolute-value, quadratic; Figure 10).

Sample efficiency (Figure 2c). We vary $n^r \in \{100, 200, 500, 1000, 2000\}$ within the nonlinear-CATE DGP ($\omega = 1.5$, $w_Z = 0$). CALM-NN maintains RMSE in the range 0.51–0.79 across all sample sizes, whereas calibration-based methods degrade sharply at small n^r : RMSE 5.32 at $n^r = 100$ compared with 0.79 for CALM-NN. Even at $n^r = 2,000$, CALM-NN retains a modest advantage (0.51 vs. 0.60). This stability arises because CALM-NN uses 10,000 OS samples for representation learning, making the quality of the learned features largely independent of RCT sample size.

Latent coupling strength (Appendix C). We vary $\alpha_U \in \{0.5, 1.0, 2.0, 3.0, 4.0\}$, controlling how much \mathbf{U} encodes information about \mathbf{V} through the shared latent. The largest margin appears at $\alpha_U = 0.5$ (RMSE 0.57 vs. 1.58); as coupling increases, calibration-based methods improve (from

1.58 to 1.27) while CALM-NN slightly increases (0.57 to 0.87), but CALM-NN remains the best method throughout. This pattern is consistent with the theory: when the latent channel is narrow, imputation is difficult and the nonlinear encoder has a greater relative advantage.

8 DISCUSSION

The experiments reveal two distinct regimes. In the baseline regime (29 settings, linear CATEs), calibration-based methods are effectively indistinguishable: margins are below 10^{-3} RMSE, and the 95% confidence interval for the gap between the best and the runner-up excludes zero in none of these settings. This validates the calibration mechanism as the dominant factor; once calibration is applied, the choice of OS-borrowing strategy has negligible impact. In the nonlinear-CATE regime (22 settings), CALM-NN wins all 22, with the advantage most pronounced at small n^r (where OS-learned representations compensate for limited RCT data), persistent across three CATE functional forms, and robust to shared-covariate signal strength. HTCE-T and HTCE-DR, which also employ neural networks and both data sources, do not achieve competitive performance in either regime, confirming that the advantage derives from CALM’s calibration-plus-alignment approach rather than neural-network flexibility alone. A semi-synthetic benchmark using IHDP covariates [Hill, 2011] confirms calibration-based equivalence: all four calibration methods achieve RMSE ≈ 0.205 , with CALM-NN at 0.23 (Appendix C, Figure 11).

9 CONCLUSION

CALM shows that CATE estimation under covariate mismatch requires only a shared representation supporting outcome prediction and calibration, not full reconstruction of missing covariates. Our risk bounds decompose the error into alignment, sufficiency, complexity, and calibration terms, revealing when embedding alignment outperforms imputation; experiments confirm these predictions. Limitations include the unobservability of the alignment quality r_ϕ^2 in practice, reliance on Lipschitz conditions, and incomplete negative-transfer protection for CALM-NN under severe dis-

tributional shift. Natural extensions include multi-source settings [Mansour et al., 2008], formal inference via de-biased ML [Chernozhukov et al., 2018], and real-world clinical applications [Heerman et al., 2024, Karlsson et al., 2025].

References

- Galen Andrew, Raman Arora, Jeff Bilmes, and Karen Livescu. Deep canonical correlation analysis. In *International Conference on Machine Learning*, pages 1247–1255, 2013.
- Amir Asiaee, Chiara Di Gravio, Cole Beck, Yuting Mei, Samhita Pal, and Jared D. Huling. Improving precision of RCT-based CATE estimation using data borrowing with double calibration. *arXiv preprint arXiv:2306.17478*, 2023.
- Susan Athey, Julie Tibshirani, and Stefan Wager. Generalized random forests. *The Annals of Statistics*, 47(2): 1148–1178, 2019.
- Peter L. Bartlett and Shahar Mendelson. Empirical minimization. *Probability Theory and Related Fields*, 135(3): 311–334, 2006.
- Shai Ben-David, John Blitzer, Koby Crammer, Alex Kulesza, Fernando Pereira, and Jennifer Wortman Vaughan. A theory of learning from different domains. *Machine Learning*, 79(1–2):151–175, 2010.
- Ioana Bica and Mihaela van der Schaar. Transfer learning on heterogeneous feature spaces for treatment effects estimation. In *Advances in Neural Information Processing Systems*, volume 35, pages 37173–37186, 2022.
- Konstantinos Bousmalis, George Trigeorgis, Nathan Silberman, Dilip Krishnan, and Dumitru Erhan. Domain separation networks. *Advances in Neural Information Processing Systems*, 29, 2016.
- David Cheng and Tianxi Cai. Adaptive combination of randomized and observational data. *arXiv preprint arXiv:2111.15012*, 2021.
- Victor Chernozhukov, Denis Chetverikov, Mert Demirer, Esther Duflo, Christian Hansen, Whitney Newey, and James Robins. Double/debiased machine learning for treatment and structural parameters. *The Econometrics Journal*, 21(1):C1–C68, 2018.
- Bénédicte Colnet, Julie Josse, Gaël Varoquaux, and Erwan Scornet. Causal effect on a target population: A sensitivity analysis to handle missing covariates. *Journal of Causal Inference*, 10(1):372–414, 2022. doi: 10.1515/jci-2021-0059.
- Bénédicte Colnet, Imke Mayer, Guanhua Chen, Awa Dieng, Ruohan Li, Gaël Varoquaux, Jean-Philippe Vert, Julie Josse, and Shu Yang. Causal inference methods for combining randomized trials and observational studies: a review. *Statistical Science*, 39(1):165–191, 2024.
- R. Dennis Cook. Fisher lecture: Dimension reduction in regression. *Statistical Science*, 22(1):1–26, 2007.
- Issa J. Dahabreh, Sarah E. Robertson, Jon A. Steingrimsson, Elizabeth A. Stuart, and Miguel A. Hernán. Extending inferences from a randomized trial to a new target population. *Statistics in Medicine*, 39(14):1999–2014, 2020. doi: 10.1002/sim.8426.
- Irina Degtiar and Sherri Rose. A review of generalizability and transportability. *Annual Review of Statistics and Its Application*, 10:501–524, 2023.
- Yaroslav Ganin, Evgeniya Ustinova, Hana Ajakan, Pascal Germain, Hugo Larochelle, François Laviolette, Mario Marchand, and Victor Lempitsky. Domain-adversarial training of neural networks. *Journal of Machine Learning Research*, 17(1):1–35, 2016.
- Trinetri Ghosh, Yanyuan Ma, and Xavier de Luna. Sufficient dimension reduction for feasible and robust estimation of average causal effect. *Statistica Sinica*, 31(2):821–842, 2021. doi: 10.5705/ss.202018.0416.
- Arthur Gretton, Karsten M. Borgwardt, Malte J. Rasch, Bernhard Schölkopf, and Alexander Smola. A kernel two-sample test. *Journal of Machine Learning Research*, 13:723–773, 2012.
- P. Richard Hahn, Jared S. Murray, and Carlos M. Carvalho. Bayesian regression tree models for causal inference: regularization, confounding, and heterogeneous effects. *Bayesian Analysis*, 15(3):965–1056, 2020.
- David R. Hardoon, Sandor Szedmak, and John Shawe-Taylor. Canonical correlation analysis: An overview with application to learning methods. *Neural Computation*, 16(12):2639–2664, 2004.
- Negar Hassanpour and Russell Greiner. Learning disentangled representations for counterfactual regression. In *International Conference on Learning Representations*, 2020.
- William J. Heerman, Russell L. Rothman, Lee M. Sanders, Jonathan S. Schildcrout, Kori B. Flower, Alan M. Delamater, Melissa C. Kay, Charles T. Wood, Rachel S. Gross, Aihua Bian, Laura E. Adams, Evan C. Sommer, H. Shonna Yin, and Eliana M. Perrin. A digital health behavior intervention to prevent childhood obesity: The Greenlight Plus randomized clinical trial. *JAMA*, 332(24): 2068–2080, 2024.
- Jennifer L. Hill. Bayesian nonparametric modeling for causal inference. *Journal of Computational and Graphical Statistics*, 20(1):217–240, 2011. doi: 10.1198/jcgs.2010.08162.

- Brian P. Hobbs, Bradley P. Carlin, Sumithra J. Mandrekar, and Daniel J. Sargent. Hierarchical commensurate and power prior models for adaptive incorporation of historical information in clinical trials. *Biometrics*, 67(3): 1047–1056, 2011.
- Joseph G. Ibrahim and Ming-Hui Chen. Power prior distributions for regression models. *Statistical Science*, 15(1): 46–60, 2000.
- Fredrik Johansson, Uri Shalit, and David Sontag. Learning representations for counterfactual inference. In *International Conference on Machine Learning*, pages 3020–3029, 2016.
- Rickard Karlsson, Piersilvio De Bartolomeis, Issa J. Dababreh, and Jesse H. Krijthe. Robust estimation of heterogeneous treatment effects in randomized trials leveraging external data. *arXiv preprint arXiv:2507.03681*, 2025.
- Edward H. Kennedy. Towards optimal doubly robust estimation of heterogeneous causal effects. *Electronic Journal of Statistics*, 17(2):3008–3049, 2023.
- David M. Kent, Jessica K. Paulus, David van Klaveren, Ralph D’Agostino, Steve Goodman, Rodney Hayward, John P. A. Ioannidis, Bray Patrick-Lake, Sally Morton, Michael Pencina, Gowri Raman, Joseph S. Ross, Harry P. Selker, Ravi Varadhan, Andrew Vickers, John B. Wong, and Ewout W. Steyerberg. The predictive approaches to treatment effect heterogeneity (PATH) statement. *Annals of Internal Medicine*, 172(1):35–45, 2020. doi: 10.7326/M18-3667.
- Michael R. Kosorok and Eric B. Laber. Precision medicine. *Annual Review of Statistics and Its Application*, 6:263–286, 2019.
- Sören R. Künzle, Jasjeet S. Sekhon, Peter J. Bickel, and Bin Yu. Metalearners for estimating heterogeneous treatment effects using machine learning. *Proceedings of the National Academy of Sciences*, 116(10):4156–4165, 2019.
- Bing Li. *Sufficient dimension reduction: Methods and applications with R*. CRC Press, 2018.
- Mingsheng Long, Yue Cao, Jianmin Wang, and Michael I. Jordan. Learning transferable features with deep adaptation networks. In *Proceedings of the 32nd International Conference on Machine Learning*, volume 37 of *JMLR Workshop and Conference Proceedings*, pages 97–105. JMLR.org, 2015.
- Yanyuan Ma and Liping Zhu. A semiparametric approach to dimension reduction. *Journal of the American Statistical Association*, 107(497):168–179, 2012.
- Yishay Mansour, Mehryar Mohri, and Afshin Rostamizadeh. Domain adaptation with multiple sources. In *Advances in Neural Information Processing Systems*, volume 21, 2008.
- Xinkun Nie and Stefan Wager. Quasi-oracle estimation of heterogeneous treatment effects. *Biometrika*, 108(2): 299–319, 2021.
- Michael Oberst, Alexander D’Amour, Minmin Chen, Yuyan Wang, David Sontag, and Steve Yadlowsky. Understanding the risks and rewards of combining unbiased and possibly biased estimators, with applications to causal inference. *arXiv preprint arXiv:2205.10467*, 2022.
- Samhita Pal, Jared D. Huling, and Amir Asiaee. Improving RCT-based CATE estimation under covariate mismatch via double calibration. *arXiv preprint arXiv:2603.17066*, 2026.
- Sinno Jialin Pan and Qiang Yang. A survey on transfer learning. *IEEE Transactions on Knowledge and Data Engineering*, 22(10):1345–1359, 2010.
- Susanne Rässler. *Statistical Matching: A Frequentist Theory, Practical Applications, and Alternative Bayesian Approaches*. Springer, 2002.
- Michael T. Rosenstein, Zvika Marx, Leslie Pack Kaelbling, and Thomas G. Dietterich. To transfer or not to transfer. In *NIPS 2005 Workshop on Transfer Learning*, 2005.
- Uri Shalit, Fredrik D. Johansson, and David Sontag. Estimating individual treatment effect: generalization bounds and algorithms. In *International Conference on Machine Learning*, pages 3076–3085, 2017.
- Claudia Shi, David M. Blei, and Victor Veitch. Adapting neural networks for the estimation of treatment effects. In *Advances in Neural Information Processing Systems*, volume 32, 2019.
- Masashi Sugiyama and Motoaki Kawanabe. *Machine Learning in Non-Stationary Environments: Introduction to Covariate Shift Adaptation*. MIT Press, 2012.
- Martin J. Wainwright. *High-Dimensional Statistics: A Non-Asymptotic Viewpoint*. Cambridge University Press, 2019.
- Rui Wang, Stephen W. Lagakos, James H. Ware, David J. Hunter, and Jeffrey M. Drazen. Statistics in medicine—reporting of subgroup analyses in clinical trials. *New England Journal of Medicine*, 357(21):2189–2194, 2007.
- Karl Weiss, Taghi M. Khoshgoftaar, and DingDing Wang. A survey of transfer learning. *Journal of Big Data*, 3(1): 9, 2016. doi: 10.1186/s40537-016-0043-6.
- Liuyi Yao, Sheng Li, Yaliang Li, Mengdi Huai, Jing Gao, and Aidong Zhang. Representation learning for treatment effect estimation from observational data. In *Advances in Neural Information Processing Systems*, volume 31, 2018.

Improving RCT-Based Treatment Effect Estimation Under Covariate Mismatch via Calibrated Alignment

Supplementary Material

A PROOFS

Proof of Theorem 1. We decompose the error in three steps: the CATE calibration layer, the augmentation error, and the assembly.

Step 1 (CATE calibration layer). By the pseudo-outcome regression framework (Asiaee et al. [2023], Theorem 6), the CATE estimation error satisfies

$$\Delta_2^2(\hat{\tau}_{\text{CALM}}, \tau^r) \leq \Delta_2^2(\mathcal{F}, \tau^r) + C_1 \left(1 + \sum_a \Delta_{2,r}^2(\hat{\mu}_a^{\text{cal}}, \bar{\mu}_a^r)\right) \mathfrak{R}_{n^r}^2(\mathcal{F}) + C_2 \frac{\log(1/\gamma)}{n^r}, \quad (17)$$

where $\bar{\mu}_a^r(\mathbf{x}^r) = \mathbb{E}[\mu_a^r(\mathbf{X}) \mid \mathbf{X}^r = \mathbf{x}^r, S = r]$ is the RCT outcome mean marginalized over \mathbf{V} , and $\hat{\mu}_a^{\text{cal}}(\mathbf{x}^r) = \hat{\mu}_a^o(\hat{\phi}^r(\mathbf{x}^r)) + \hat{\delta}_a^t(\hat{\phi}^r(\mathbf{x}^r))$ is the calibrated prediction from Stage 2. The first term is the approximation error of \mathcal{F} ; the second captures how the quality of the CMO estimate amplifies the CATE estimation error. Cross-fitting ensures that the nuisance estimates $\hat{\mu}_a^{\text{cal}}$ are independent of the pseudo-outcome regression sample, allowing us to bound the stochastic term via Rademacher complexity and a concentration inequality.

Step 2 (Augmentation error decomposition). The per-arm augmentation error $\Delta_{2,r}^2(\hat{\mu}_a^{\text{cal}}, \bar{\mu}_a^r)$ is further decomposed into four terms. For any RCT unit with covariates \mathbf{x}^r , let $\mathbf{v}^* \sim P(\mathbf{V} \mid \mathbf{X}^r = \mathbf{x}^r, S = r)$ denote the (unobserved) OS-only covariate.

$$\begin{aligned} \hat{\mu}_a^{\text{cal}}(\mathbf{x}^r) - \bar{\mu}_a^r(\mathbf{x}^r) &= \underbrace{\hat{\mu}_a^o(\hat{\phi}^r) + \hat{\delta}_a^t(\hat{\phi}^r) - \tilde{\mu}_a^r(\hat{\phi}^r)}_{\text{(I): estimation}} + \underbrace{\tilde{\mu}_a^r(\hat{\phi}^r) - \tilde{\mu}_a^r(\hat{\phi}^o(\mathbf{x}^{o,*}))}_{\text{(II): alignment}} \\ &\quad + \underbrace{\tilde{\mu}_a^r(\hat{\phi}^o(\mathbf{x}^{o,*})) - \mu_a^r(\mathbf{x}^r, \mathbf{v}^*)}_{\text{(III): sufficiency}} + \underbrace{\mu_a^r(\mathbf{x}^r, \mathbf{v}^*) - \bar{\mu}_a^r(\mathbf{x}^r)}_{\text{(IV): marginalization}}, \end{aligned}$$

where $\hat{\phi}^r = \hat{\phi}^r(\mathbf{x}^r)$ is shorthand.

Term (I): By cross-fitting, $\hat{\mu}_a^o$ is estimated on independent OS data and $\hat{\delta}_a^t$ on independent RCT data. Standard empirical process arguments (e.g., Bartlett and Mendelson [2006], Wainwright [2019]) bound $\mathbb{E}[(\hat{\mu}_a^o(\mathbf{h}) + \hat{\delta}_a^t(\mathbf{h}) - \tilde{\mu}_a^r(\mathbf{h}))^2] \leq C(\mathfrak{N}_{n^o}^2(\mathcal{M}_a^o) + \mathfrak{N}_{n^r}^2(\mathcal{D}_a))$ uniformly over the support of the embeddings.

Term (II): By Assumption 3, $\tilde{\mu}_a^r = \tilde{\mu}_a^o + \delta_a$. Both $\tilde{\mu}_a^o$ and δ_a are Lipschitz (Assumption 4), so

$$|\tilde{\mu}_a^r(\hat{\phi}^r) - \tilde{\mu}_a^r(\hat{\phi}^o(\mathbf{x}^{o,*}))| \leq (L_\mu + L_\delta) \|\hat{\phi}^r - \hat{\phi}^o(\mathbf{x}^{o,*})\|.$$

Squaring and taking expectations yields the alignment term $(L_\mu + L_\delta)^2 r_\phi^2$.

Term (III): By the triangle inequality,

$$|\tilde{\mu}_a^r(\hat{\phi}^o(\mathbf{x}^{o,*})) - \mu_a^r(\mathbf{x}^r, \mathbf{v}^*)| \leq |\tilde{\mu}_a^r(\hat{\phi}^o(\mathbf{x}^{o,*})) - \tilde{\mu}_a^r(\hat{\phi}^r)| + |\tilde{\mu}_a^r(\hat{\phi}^r) - \mu_a^r(\mathbf{x}^r, \mathbf{v}^*)|.$$

The first term is bounded by $(L_\mu + L_\delta) \|\hat{\phi}^r(\mathbf{x}^r) - \hat{\phi}^o(\mathbf{x}^{o,*})\|$ by Lipschitzness (Assumption 4). The second term is bounded by ϵ_{suff}^2 by Assumption 2 with $s = r$ (since $\hat{\phi}^r$ is evaluated on RCT units). Squaring and taking expectations yields a bound of order $\epsilon_{\text{suff}}^2 + (L_\mu + L_\delta)^2 r_\phi^2$.

Term (IV): By Jensen's inequality, $\mathbb{E}[(\mu_a^r(\mathbf{x}^r, \mathbf{v}^*) - \bar{\mu}_a^r(\mathbf{x}^r))^2 \mid \mathbf{X}^r = \mathbf{x}^r, S = r] = \text{Var}(\mu_a^r(\mathbf{X}) \mid \mathbf{X}^r = \mathbf{x}^r, S = r)$. Since the CATE target already marginalizes over \mathbf{V} (Eq. 1), this variance enters the irreducible error and does not affect the estimation bound.

Combining Terms (I)–(III) via the Cauchy–Schwarz inequality:

$$\Delta_{2,r}^2(\hat{\mu}_a^{\text{cal}}, \bar{\mu}_a^r) \leq C[\epsilon_{\text{suff}}^2 + (L_\mu + L_\delta)^2 r_\phi^2 + \mathfrak{N}_{n^o}^2(\mathcal{M}_a^o) + \mathfrak{N}_{n^r}^2(\mathcal{D}_a)]. \quad (18)$$

Step 3 (Assembly). Substituting (18) into (17), absorbing the multiplicative factor into constants, and summing over arms yields (15). The $\log(1/\gamma)/n^r$ term arises from a union bound and Bernstein-type concentration applied to the empirical process in the CATE calibration stage. \square

B ALIGNMENT OBJECTIVE DETAILS

Throughout this section we write $\mathbf{w}_j^o = \hat{\phi}^o(\mathbf{X}_j^o)$ for the frozen OS embeddings and $\mathbf{w}_i^r = \phi^r(\mathbf{X}_i^r)$ for the learnable RCT embeddings, both in \mathbb{R}^d .

B.1 DISTRIBUTION-MATCHING ALIGNMENT (MMD)

Instantiating (13) with the Gaussian RBF kernel $k(\mathbf{w}, \mathbf{w}') = \exp(-\|\mathbf{w} - \mathbf{w}'\|^2 / (2\sigma^2))$ and expanding the squared RKHS norm yields the unbiased U-statistic estimate

$$\begin{aligned} \mathcal{L}_{\text{MMD}} = & \frac{1}{n^o(n^o-1)} \sum_{\substack{j, j' \in \text{OS} \\ j \neq j'}} \exp\left(-\frac{\|\mathbf{w}_j^o - \mathbf{w}_{j'}^o\|^2}{2\sigma^2}\right) - \frac{2}{n^o n^r} \sum_{j \in \text{OS}} \sum_{i \in \text{RCT}} \exp\left(-\frac{\|\mathbf{w}_j^o - \mathbf{w}_i^r\|^2}{2\sigma^2}\right) \\ & + \frac{1}{n^r(n^r-1)} \sum_{\substack{i, i' \in \text{RCT} \\ i \neq i'}} \exp\left(-\frac{\|\mathbf{w}_i^r - \mathbf{w}_{i'}^r\|^2}{2\sigma^2}\right). \end{aligned} \quad (19)$$

The bandwidth σ is set via the median heuristic: $\sigma = \sqrt{\text{median}\{\|\mathbf{w}_i - \mathbf{w}_j\|^2 : i \neq j\}}$, computed over the pooled embeddings from both sources [Gretton et al., 2012]. Since $\hat{\phi}^o$ is frozen, only the cross-term and the RCT–RCT term contribute gradients with respect to ϕ^r .

B.2 Z-CONDITIONED CONTRASTIVE ALIGNMENT

The contrastive loss (14) pairs each RCT unit i with its OS neighbours $N_i = \{j \in \text{OS} : \|\mathbf{Z}_j - \mathbf{Z}_i\| \leq \varepsilon\}$ in shared-covariate space and penalizes the squared embedding distance:

$$\mathcal{L}_{\text{contr}} = \frac{1}{n^r} \sum_{i \in \text{RCT}} \frac{1}{|N_i|} \sum_{j \in N_i} \|\mathbf{w}_j^o - \mathbf{w}_i^r\|^2. \quad (20)$$

This objective is already in closed form; the neighbourhood radius ε trades off bias (large ε matches dissimilar units) against variance (small ε yields few or no neighbours).

B.3 ADVERSARIAL DOMAIN ALIGNMENT

Following Ganin et al. [2016], we introduce a domain discriminator $g_\omega : \mathbb{R}^d \rightarrow [0, 1]$ trained to distinguish OS from RCT embeddings, while the RCT encoder ϕ^r is trained to fool it. Let $s_j = 1$ for OS units and $s_i = 0$ for RCT units. The adversarial alignment objective is

$$\mathcal{L}_{\text{adv}} = -\frac{1}{n^o} \sum_{j \in \text{OS}} \log g_\omega(\mathbf{w}_j^o) - \frac{1}{n^r} \sum_{i \in \text{RCT}} \log(1 - g_\omega(\mathbf{w}_i^r)), \quad (21)$$

which is maximized over ω and minimized over ϕ^r via a gradient reversal layer [Ganin et al., 2016]. At the minimax equilibrium, $g_\omega \equiv 1/2$, implying that the embedding distributions are indistinguishable. We do not use adversarial alignment in our experiments because (i) it introduces a second network and alternating optimization, making training less stable, and (ii) preliminary runs showed no improvement over the simpler MMD objective; we include it here for completeness.

B.4 IMPLEMENTATION NOTES

In our CALM-NN implementation, we use the MMD objective (19) as the default alignment loss (`align_mode = mmd`). We additionally implement a *conditional-mean alignment* variant (`align_mode = cond_mean`), which fits a ridge regression $\mathbf{Z} \mapsto \mathbb{E}[\hat{\phi}^o(\mathbf{Z}, \mathbf{V}) \mid \mathbf{Z}]$ on the OS and uses the predicted embeddings as alignment targets for ϕ^r :

$$\mathcal{L}_{\text{cond}} = \frac{1}{n^r} \sum_{i \in \text{RCT}} \|\mathbf{w}_i^r - \hat{h}(\mathbf{Z}_i)\|^2, \quad \hat{h} = \arg \min_{h \in \mathcal{H}_{\text{ridge}}} \frac{1}{n^o} \sum_{j \in \text{OS}} \|h(\mathbf{Z}_j) - \mathbf{w}_j^o\|^2 + \alpha \|h\|^2. \quad (22)$$

This variant avoids kernel bandwidth selection and is computationally cheaper but assumes a linear relationship between \mathbf{Z} and the OS embeddings. The alignment weight λ is annealed during Stage 2 training: held constant for the first 60% of epochs, then linearly decayed to 0.2λ over the remaining 40%.

C ADDITIONAL EXPERIMENTAL RESULTS

C.1 BASELINE REGIME

This subsection reports additional sweeps from the baseline (linear-CATE) regime described in Section 7. The DGP uses $p_z = 30$, $p_u = 10$, $p_v = 20$, linear outcomes, and default parameters $n^r = 500$, $n^o = 10,000$, $\sigma_V^2 = 1.0$, $d_{\text{true}} = 5$, shift

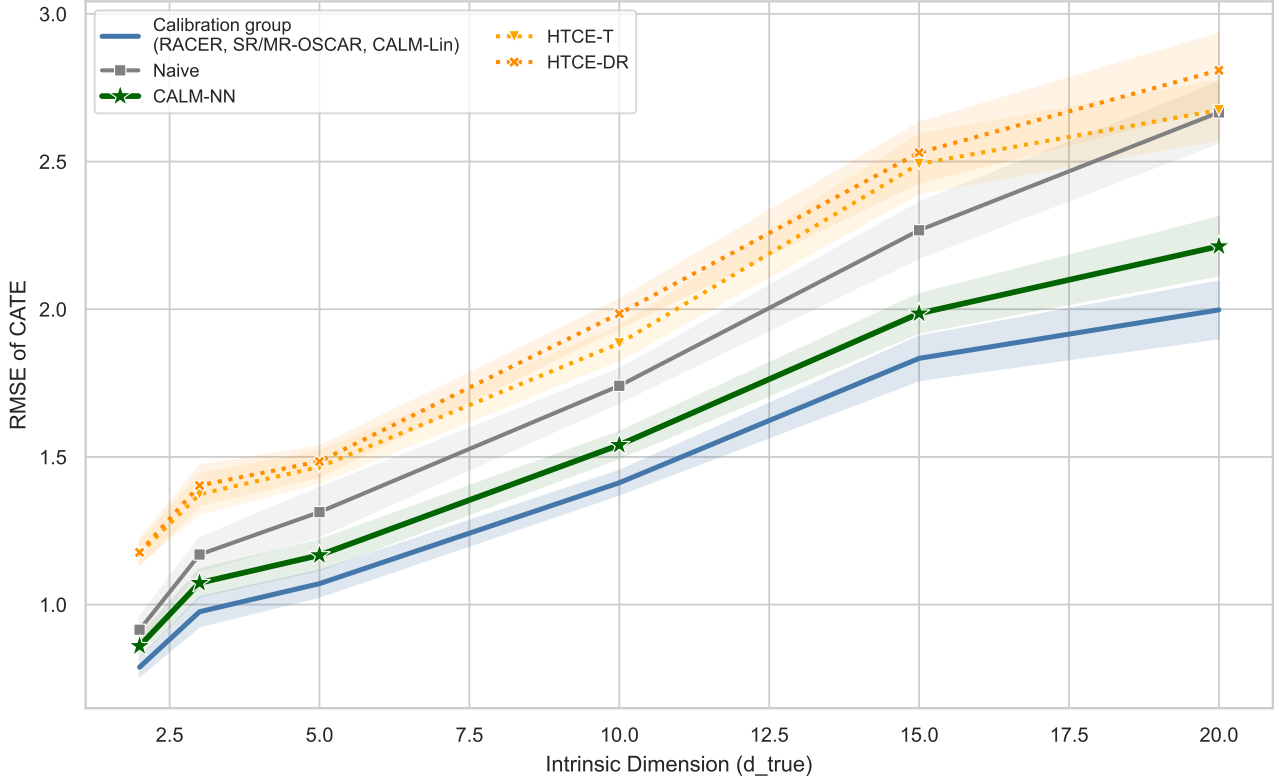


Figure 3: RMSE of CATE estimation as a function of intrinsic dimension d_{true} , with $\sigma_V^2 = 1.0$, $n^r = 500$, and linear outcome model. Mean over 20 replicates. Blue band: calibration-group envelope (see Figure 2 caption). No single method dominates uniformly across intrinsic dimensions.

magnitude 0.5. Each figure varies one factor while holding the rest at defaults. Mean RMSE is computed over 20 replicates. Across all settings, the four calibration-based methods (RACER, SR-OSCAR, MR-OSCAR, CALM-Lin) remain effectively indistinguishable (pairwise RMSE differences below 10^{-3}).

C.2 NONLINEAR-CATE REGIME

This subsection provides additional sweeps from the nonlinear-CATE regime described in Section 7.5. The DGP uses a shared-latent structure: U and V share a 5-dimensional latent factor ($\sigma_U^2 = \sigma_V^2 = 0.1$), outcomes depend only on V ($w_Z = w_U = 0$, $w_V = 2$), and the CATE takes a sinusoidal form with frequency ω . Mean RMSE is computed over 20 replicates. CALM-NN attains the lowest RMSE in all settings reported here.

Under absolute-value CATEs, CALM-NN achieves RMSE 2.41 versus 2.86 for the best calibration-based method (margin 0.45); under quadratic CATEs, 15.60 versus 18.83 (margin 3.23). The quadratic form is difficult for all methods due to the unbounded square function, but CALM-NN still attains the lowest RMSE (sinusoidal: 0.63 vs. 1.18, margin 0.55).

C.3 SEMI-SYNTHETIC BENCHMARK

We construct a semi-synthetic benchmark from the IHDP dataset [Hill, 2011], splitting covariates into Z , U , and V and bootstrap-sampling units to form OS and RCT datasets. Outcomes follow a structural model with a treatment effect $\tau(X^r)$ and an RCT-only shift $\delta_a^r(Z)$ to induce domain mismatch. All eight methods from Section 7 are evaluated over 50 replicates. Results confirm the calibration-based equivalence observed in the linear-CATE simulations: all four calibration methods achieve $\text{RMSE} \approx 0.205$, with CALM-NN at 0.23 (Figure 11).

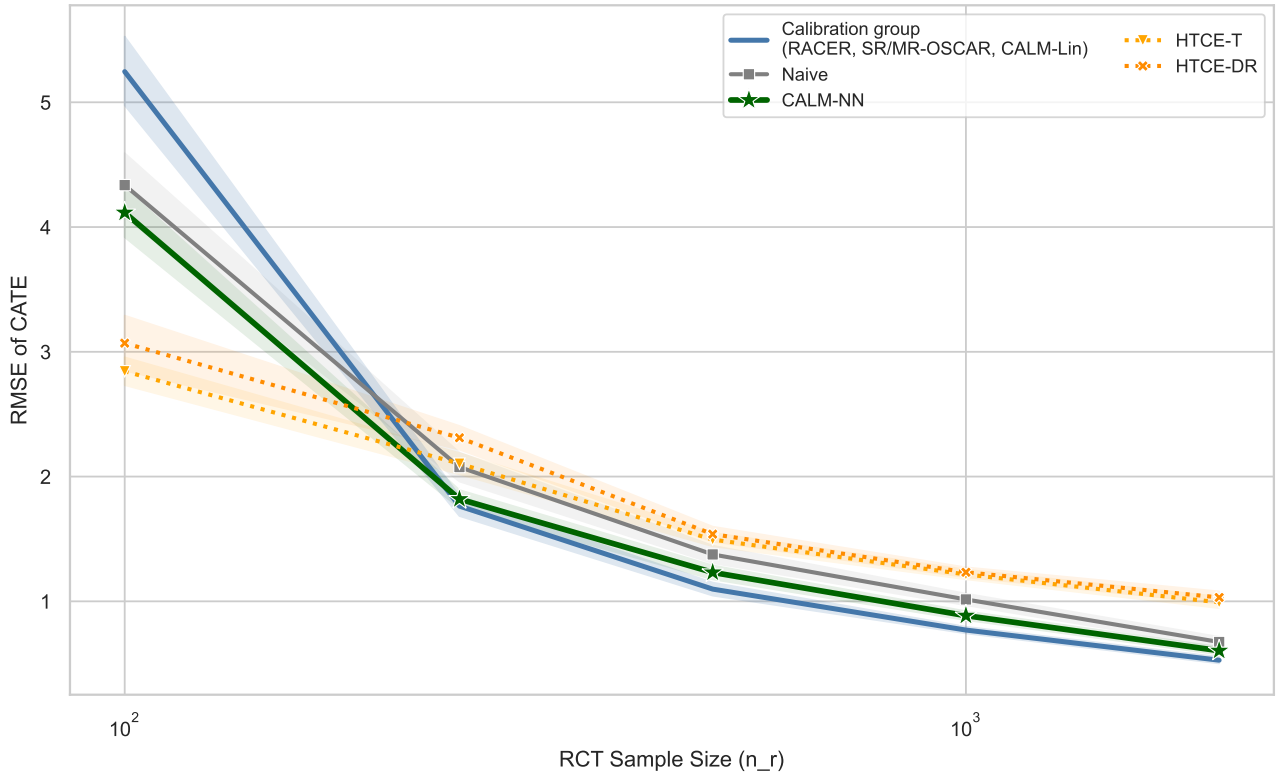


Figure 4: RMSE of CATE estimation as a function of RCT sample size n^r , with $n^o = 10,000$ fixed, $\sigma_V^2 = 1.0$, $d_{\text{true}} = 5$, and linear outcome model. Mean over 20 replicates. Blue band: calibration-group envelope (see Figure 2 caption). HTCE methods perform best at the smallest n^r , while calibration-based methods converge as n^r grows.

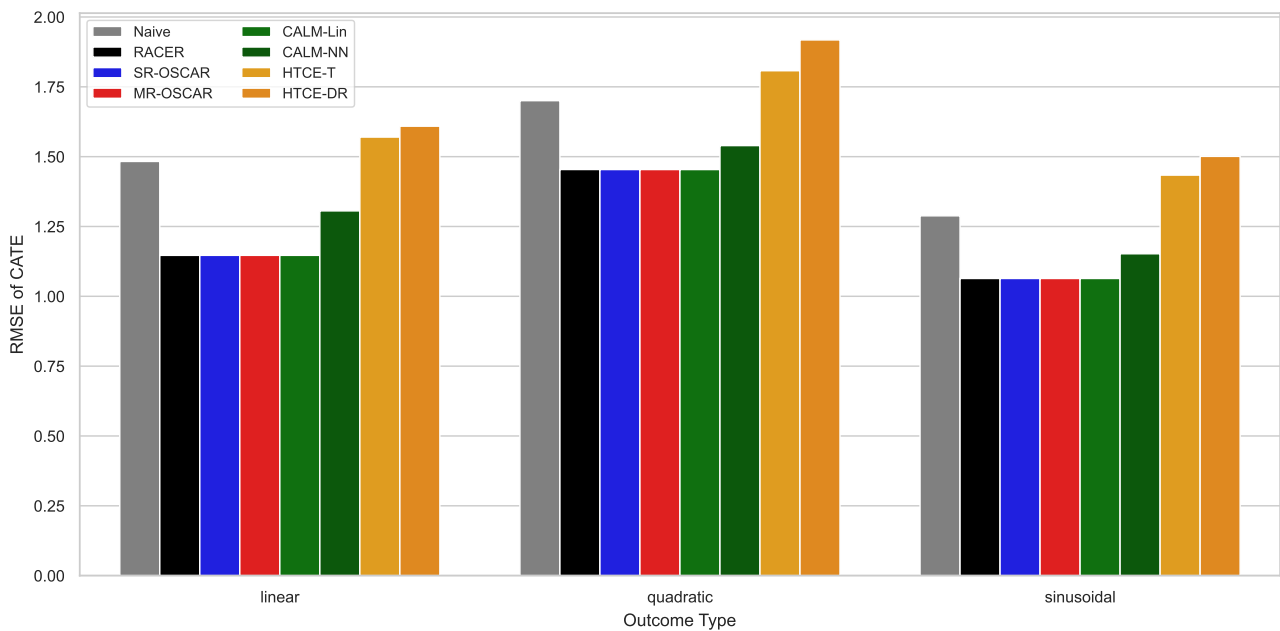


Figure 5: RMSE across outcome model types (linear, quadratic, sinusoidal), with $\sigma_V^2 = 1.0$, $n^r = 500$, $d_{\text{true}} = 5$. Bars show mean RMSE over 20 replicates. The best method depends on the outcome type.

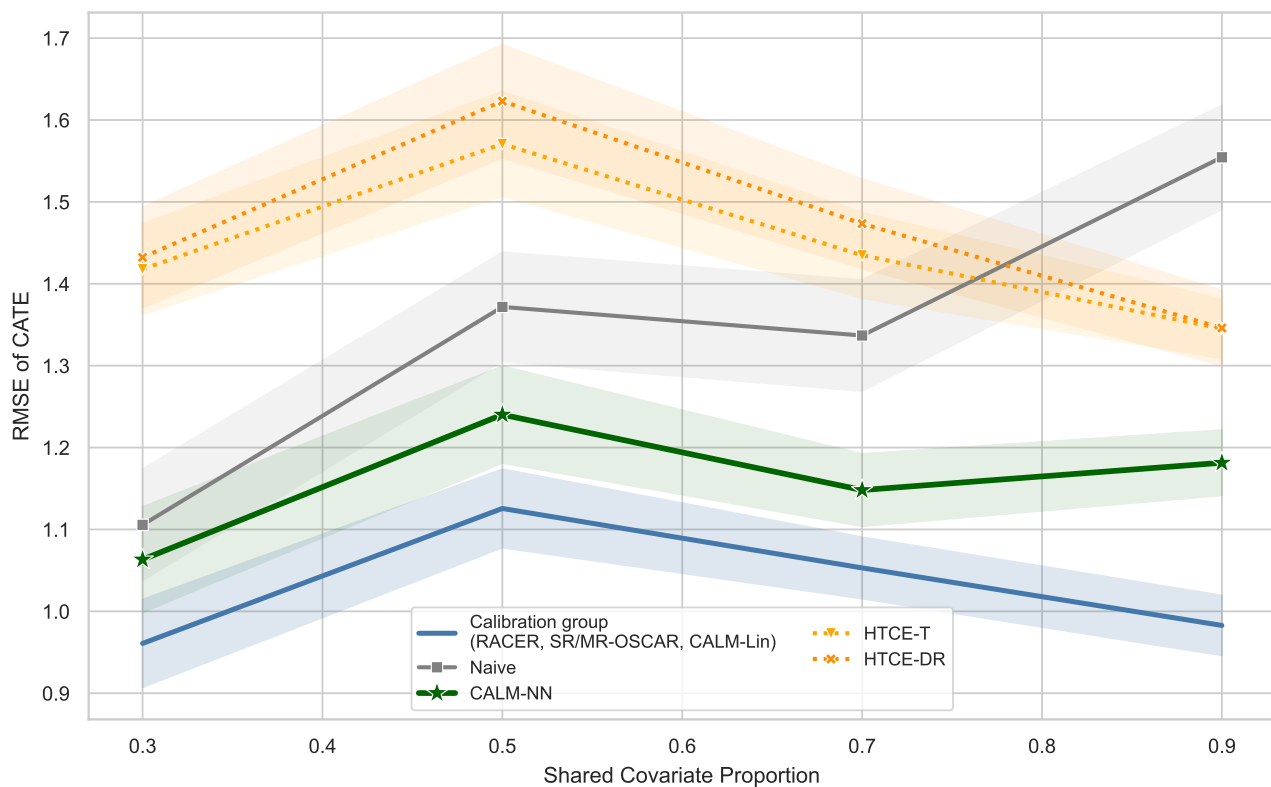


Figure 6: RMSE as a function of shared covariate proportion $p_z/(p_z + p_v)$, with $\sigma_V^2 = 1.0$, $n^r = 500$, $d_{\text{true}} = 5$, and linear outcome model. Mean over 20 replicates. Blue band: calibration-group envelope (see Figure 2 caption). Performance improves as shared proportion increases and the mismatch problem weakens.

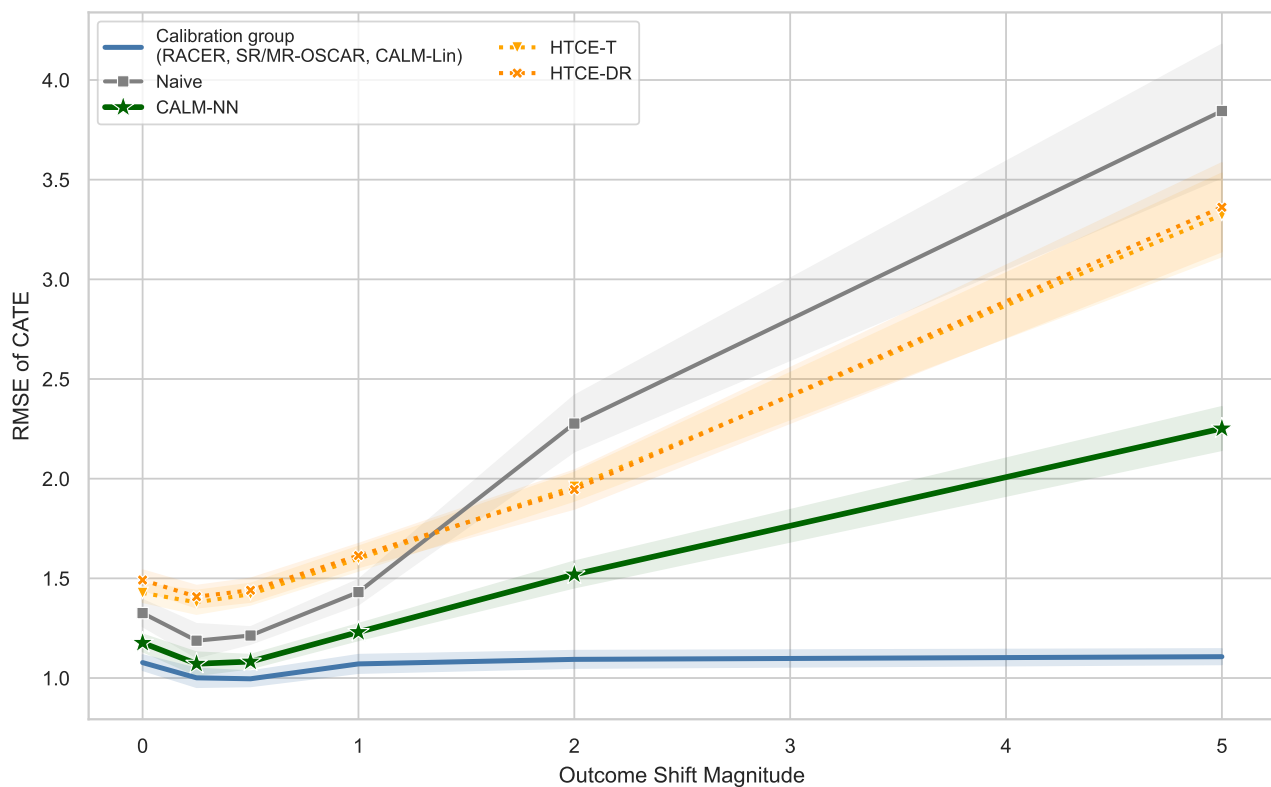


Figure 7: RMSE under increasing outcome shift between OS and RCT, with $\sigma_V^2 = 1.0$, $n^r = 500$, and linear outcome model. Mean over 20 replicates. Blue band: calibration-group envelope (see Figure 2 caption). Calibration-based methods remain stable under shift, while Naive and HTCE methods inflate under large shift.

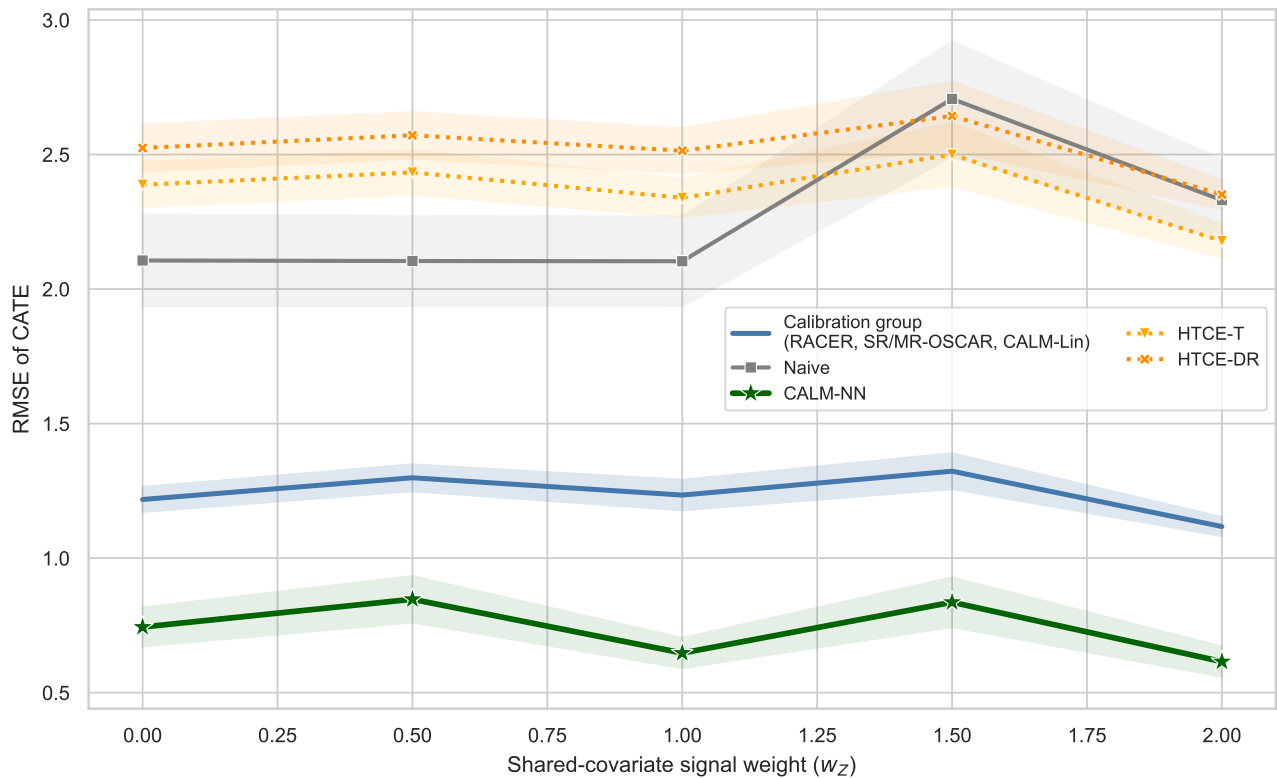


Figure 8: RMSE as a function of shared-covariate signal weight w_Z , with $w_V = 2$, $\omega = 1.5$, and the nonlinear-CATE DGP. Mean over 20 replicates. Blue band: calibration-group envelope (see Figure 2 caption). CALM-NN's advantage persists even when Z contributes substantially to the outcome signal.

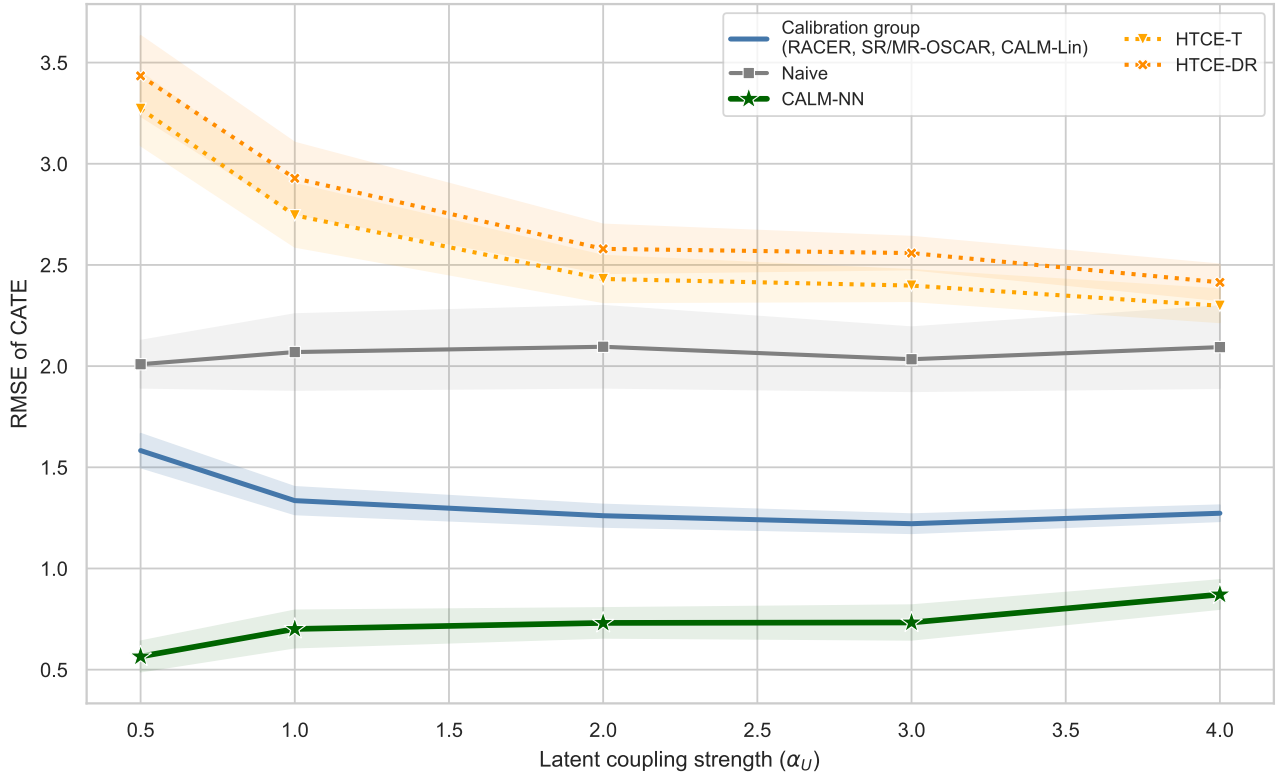


Figure 9: RMSE as a function of latent coupling strength α_U , which controls how much U encodes information about V through shared latent factors. Nonlinear-CATE DGP with $\omega = 1.5$, $w_Z = 0$. Mean over 20 replicates. Blue band: calibration-group envelope (see Figure 2 caption).

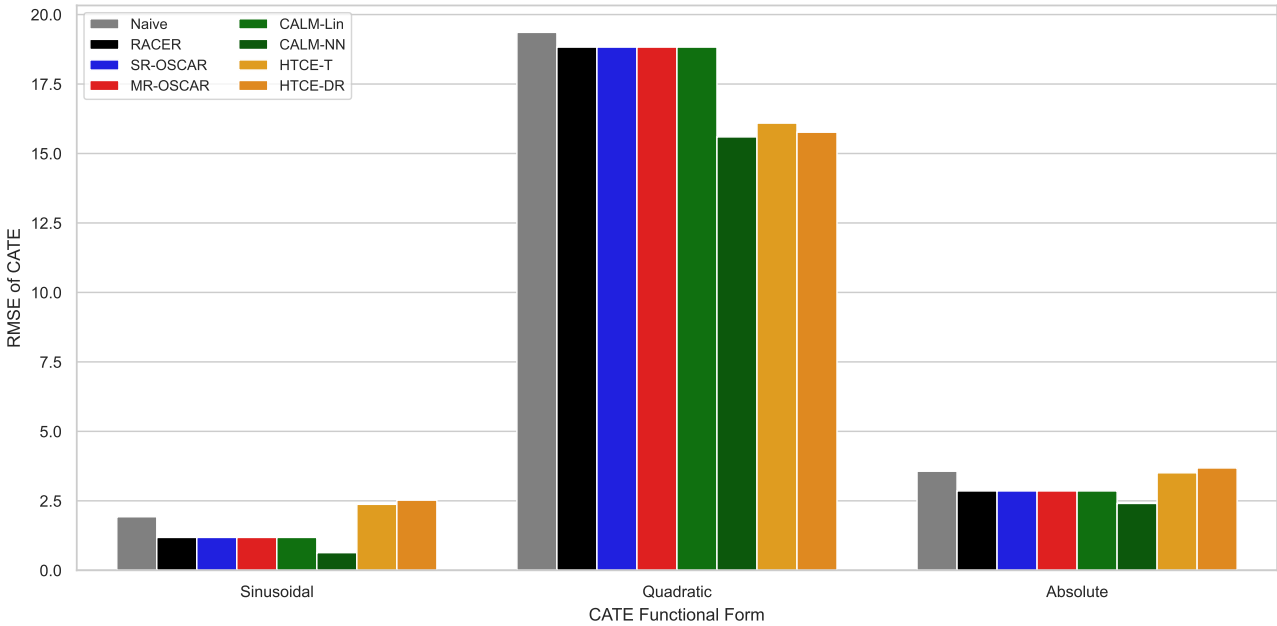


Figure 10: RMSE across three nonlinear CATE functional forms (sinusoidal, quadratic, absolute value) in the nonlinear-CATE DGP ($\omega = 1.5$, $w_Z = 0$). Bars show mean RMSE over 20 replicates. CALM-NN (dark green) achieves the lowest RMSE across all three forms.

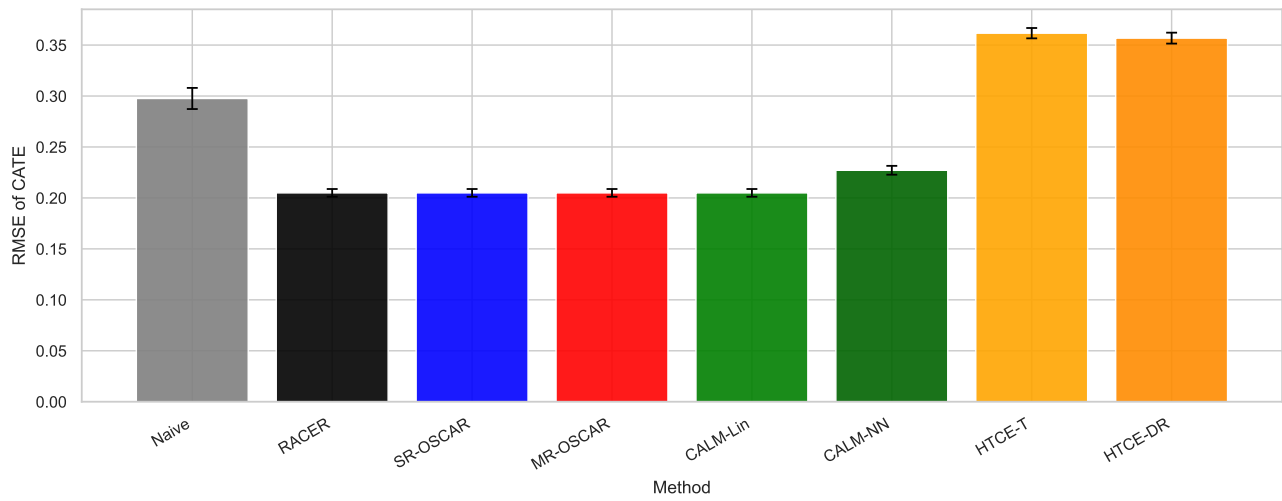


Figure 11: Semi-synthetic benchmark using IHDP covariates: mean RMSE of CATE estimation over 50 replicates (error bars: ± 1 SE).